

Supporting Information for

Chemical mapping of the surface interactome of PIEZO1 identifies
CADM1 as a modulator of channel inactivation

Anna K. Koster^{a,b}, Oleg Yarishkin^a, Adrienne E. Dubin^a, Jennifer M. Kefauver^a,
Ryan A. Pak^a, Benjamin F. Cravatt^{*b}, Ardem Patapoutian^{*a}

Corresponding author(s): Ardem Patapoutian, Benjamin F. Cravatt

Email: ardem@scripps.edu , cravatt@scripps.edu

This PDF file includes:

Supporting Materials and Methods
Figures S1 to S5
Tables S1 to S6
Appendix I: Electrophysiology screen data, as summarized in Table S1
Appendix II: cDNA library information
Appendix III: Calcium imaging screen data
Supplementary File 2: Spreadsheet Legend
SI References

Other supporting materials for this manuscript include the following:

Supplementary File 2 (proteomics summary data*)

*Raw data for TMT mass spectrometry experiments have been deposited in
ProteomeXchange Consortium(1) via the PRIDE partner repository(2): Accession No.
PXD054618.

Supporting Information: Materials and Methods

Molecular biology: *Subcloning of cDNA library.* For expression studies, cDNA sequences contained in Gateway pDONR vector backbone were subcloned as fusion constructs into mammalian expression vectors with a C-terminal mCherry tag (Addgene, Plasmid#31907) via the LR recombination reaction. Briefly, the destination vector was amplified by transforming into One Shot® ccdB Survival 2 T1^R Chemically Competent *E. coli* (Life Technologies, Cat#A10460) using chloramphenicol (25 µg/mL) and kanamycin (50 µg/mL) in Luria broth (LB) or agar for antibiotic selection. Plasmid DNA was purified from the bacterial pellet using the QIAprep spin miniprep kit (Qiagen, Cat#27106), according to manufacturer instructions. For the LR reaction, donor vector (1 µL, 100 ng) was combined with destination vector (1 µL, 150 ng) and 1 µL Gateway™ LR Clonase™ II enzyme mix (Life Technologies, Cat#11791020) in 7 µL TE buffer, pH 8.0 (10 mM Tris-HCl, 1 mM EDTA). Following overnight incubation at room temperature, 2 µL of the recombination reaction were transformed into 20 µL NEB 10-beta competent *E. coli* (New England Biolabs, Cat#C3019H) and selected with kanamycin (50 µg/mL).

Subcloning of untagged cDNAs into IRES-tdTomato or IRES-mCherry expression vectors was accomplished by polymerase chain reaction (PCR)-based cloning. Briefly, forward and reverse PCR amplification primers were designed for each gene containing a 6-basepair leader sequence to assist with restriction digest (5'-3' Forward leader: TAAGCA, Reverse leader: TGCTTA) the appropriate restriction site, and a hybridization sequence complementary to the sequence to be amplified. The length of the hybridization sequence was optimized to match the annealing temperatures of the forward and reverse primers as closely as possible. If not already included in the expression vector, a Kozak sequence (GCCACCATGG) for strong initiation of translation was incorporated into the forward primer, and a stop codon (TAA or TAG) was incorporated into the reverse primer. Genes were amplified via PCR with Phusion High-Fidelity DNA polymerase (Fisher Scientific, Cat#F530L) in HF Phusion buffer, according to suggested manufacturer thermocycling conditions. Annealing temperatures were determined using the NEB T_m Calculator tool (<https://tmcalculator.neb.com>) and a 30 seconds-per-kilobase extension time. PCR products were purified using the QIAQuick PCR purification kit (Qiagen, Cat#28104). The purified PCR product and recipient plasmid backbone were digested with the appropriate pair of restriction enzymes (Thermo Scientific, FastDigest) and loaded onto a 1% agarose gel containing SYBR™ safe DNA gel stain (Life Technologies, Cat#S33102) to verify correct amplicon and recipient plasmid backbone lengths (using NEB 1 kb Plus DNA ladder, Cat#N3200S). The digested PCR product and recipient plasmid backbone were excised from the agarose gel and purified using the ZymoClean Gel DNA recovery kit (Zymo Research, Cat#D4002). The purified DNA fragments were ligated in a 3:1–5:1 ratio of PCR insert to backbone recipient plasmid using T4 DNA ligase (New England Biolabs, Cat#M0202L), according to the suggested manufacturer protocol. Following a 10-minute incubation at room temperature, 2 µL of the recombination reaction were transformed into 20 µL of NEB 10-beta competent *E. coli* (New England Biolabs, Cat#C3019H) and selected with the appropriate antibiotic selection marker (kanamycin or carbenicillin).

Additional PIEZO construct information. The PIEZO1-BBS (blade) construct contains an I → M single nucleotide polymorphism (SNP) in the *Piezo1* coding sequence at position 105 (in the canonical sequence without the BBS tag), and *Piezo1*-BBS (cap) contains an L → P SNP at position 574 relative to the canonical mPIEZO1 sequence. These constructs traffic to the plasma membrane normally and are functionally similar to canonical mPIEZO1, as previously characterized by the Grandl lab(3) (and confirmed by our lab). Both *Piezo1* constructs reside in the pcDNA3.1(–) backbone and are ampicillin resistant, and Kv1.2-BBS-S1-S2-IRES-GFP is resistant to kanamycin.

Cell surface proximity labeling of PIEZO1. Prior to starting the experiment, a radical quenching solution and diluted solution of hydrogen peroxide were freshly prepared and kept on ice. The quenching solution was composed of 5 mM Trolox ((±)-6-hydroxy-2,5,7,8-tetramethyl-chromane-2-carboxylic acid, CAS# 53188-07-1, Sigma-Aldrich, Lot# BCBW5446, from a 500 mM stock solution in DMSO), 10 mM L-ascorbic acid sodium salt (ACROS, Fisher Scientific, Catalog#AC352680050, CAS#134-03-2, from a 1M stock in water), and 10 mM sodium azide (ReagentPlus CAS#26628-22-8, #S2002-5g, Sigma-Aldrich from a 1 M stock in water) in DPBS (Gibco, Cat#14190-136).

Hydrogen peroxide (30% w/w in water, Sigma-Aldrich Cat#H1009-100mL, CAS#7722-84-1) was diluted to 0.3% in deionized water and kept on ice until addition.

To append HRP to PIEZO1 channels on the cell surface, each 15-cm dish of cells was first incubated with 8 μ L (500 μ g/mL) of α -bungarotoxin biotin-XX conjugate stock (Invitrogen, Cat#B1196) per 20 mL media at 37 °C for 30 min (final concentration of 0.2 μ g/mL, 1:5000, ~25 nM). At the end of the incubation, cells were washed with 2 \times 20-mL DPBS (Gibco, Cat#14190-136) and incubated with 15 mL of complete DMEM media containing 15 μ L (1 mg/mL stock solution in DPBS) of streptavidin horseradish peroxidase (strp-HRP, Invitrogen Life Technologies Cat#S911, 1:1000 dilution) for 20–30 minutes at room temperature. The strp-HRP solution was gently rocked over the cells, manually, two times during the incubation. Cells were washed with 3 \times 20 mL DPBS to remove any unbound strp-HRP. For proximity labeling, a 250 mM stock of biotin phenol (BP, CAS#41994-02-9, APExBIO Cat#A8011, Boston, MA) was prepared in cell culture grade DMSO and added to 20 mL of complete DMEM (final concentration 250 μ M). The BP-DMEM (20 mL) was added to the plate followed by immediate addition of 200 μ L of 0.3% hydrogen peroxide (final concentration during labeling is 0.003%). The plate was gently rocked back and forth, manually, to evenly disperse H₂O₂ and then incubated for exactly 30 seconds. After 30 s, DMEM-BP was gently removed and replaced with 10 mL of ice-cold quencher solution for a total labeling time of 45–60 s prior to radical quenching. After 20–60 s, the solution was removed and replaced with an additional 15 mL of fresh, ice-cold quenching solution. The plate was placed on ice until cell collection. For labeling in the presence of the PIEZO1 agonist Yoda1, 100 μ L of 2 mM Yoda1 in DMSO (TOCRIS, Cat.#558610, CAS#448947-81-7) or 100 μ L of DMSO vehicle control was added to 20 mL of the BP-DMEM solution and vigorously vortexed (10 μ M final concentration of Yoda1 during labeling). Yoda1 is poorly soluble in aqueous solutions, so it is critical to perform this step just before addition to the plate to ensure that Yoda1 does not precipitate prior to addition. To keep the timing consistent, plates were treated with α -bungarotoxin biotin and strp-HRP in pairs, and biotinylation was performed one plate at a time. To maintain integrity of cell surface proteins, cells were mechanically dissociated with a cell scraper and washed with additional cold DPBS for collection in a Falcon tube. Cells were pelleted at 80 \times g for 3 minutes at 4 °C. Each cell pellet was gently resuspended in 5-mL of ice cold DPBS, centrifuged again, and resuspended a final time in 13.5 mL of cold DPBS (0.5 mL of this was retained for Western blot to verify biotinylation prior to MS). The cells were pelleted at 80 \times g for 3 minutes, the supernatant was removed, and the cell pellet was flash frozen in liquid nitrogen prior to storage at –80 °C.

Western blot for characterization of PIEZO1-BBS (cap) stable cell line. Cells were lysed with 1% NP-40 lysis buffer (25 mM Tris-HCl pH 7.4; 150 mM NaCl; 10% glycerol; 1% Nonidet P-40 in water) containing one protease inhibitor cocktail tablet (Roche, cOmplete ULTRA tablets, Mini, EDTA-free, Cat#5892791001) per 10 mL of lysis buffer. Cell pellets were kept on ice and resuspended in lysis buffer by vortexing, followed by probe sonication for 10 pulses at 4 °C (40%, output 4). Samples were centrifuged at 16,300 \times g for 10 minutes at 4 °C, and the supernatant was retained for protein quantification. Protein was quantified using a DC absorbance assay (BioRAD Cat#5000112) and serial dilutions of a 2 mg/mL bovine serum albumin protein standard, according to the manufacturer instructions. Protein concentrations were normalized and loaded (18–45 μ g total protein per lane) onto a 4–20% Novex Tris-Glycine gradient gel (Invitrogen, Cat#XP04202BOX) with denaturing 1×Laemmli loading buffer (250 mM Tris-HCl pH 6.8; 8% sodium dodecyl sulfate; 10% glycerol; 20% β -mercaptoethanol; ~5 mM bromphenol blue). Samples were not heated prior to gel loading to avoid membrane protein aggregation. The gel was run for 1.5 h at 150 V. Proteins were transferred from the gel to an activated 0.2 μ m PVDF membrane (BioRad Cat#1620177) with Towbin transfer buffer (25 mM Tris, 192 mM glycine, 20% MeOH v/v, pH 8.3) for 1.5 h at 400 mA constant current. Following transfer, the PVDF membrane was incubated in a TBS-T buffer (20 mM Tris-HCl pH 7.6, 150 mM NaCl with 0.1% Tween 20) containing 5% milk (Research Products International, Cat#M17220-1000) for 1 h at room temperature. Following block, the membrane was incubated with strp-HRP antibody (Invitrogen Life Technologies Cat#S911, 1:5000) overnight (16 h) at 4 °C. Before developing, the membrane was washed 3 \times with TBS-T buffer for 5 minutes on a rocker. Biotinylation was visualized with SuperSignal West pico PLUS (Thermo Scientific, Cat#34579), using a BioRad ChemiDoc XRS.

Mass spectrometry. *Preliminary method development.* As a proof of concept, we transiently expressed two PIEZO1 constructs with the BBS tag inserted into either the extracellular cap or distal blade. Both of these constructs are expressed normally at the plasma membrane and behave like wild-type PIEZO1(3). As controls, we additionally expressed a BBS-tagged voltage-gated potassium channel (K_v1.2-BBS)(3) and a generic plasma membrane targeted HRP (HRP-TM, Addgene plasmid #44441)(4) that should be non-specifically expressed over the entire cell surface. Because the radius of biotinylation is akin to a contour map in which the extent of biotinylation drops off as a function of distance from HRP, we hypothesized that ratiometric analysis of proteins enriched more strongly by PIEZO over other membrane protein controls are more likely to be specific interaction partners. While roughly the same set of proteins was captured across datasets, we found that quantitative prioritization of protein interaction candidates proved challenging based on our initial assumptions. First, we found that ratiometric evaluation and ranking of proteins enriched by PIEZO1-BBS compared to K_v1.2-BBS and HRP-TM was inconsistent among replicates, with HRP-TM completely overwhelming the PIEZO1-BBS signal and K_v1.2-BBS producing a lower signal across the proteome, presumably due to lower expression at the plasma membrane. In addition to the challenges of normalizing the plasma membrane expression of each construct, PIEZO1 and K_v1.2 are composed of multiple subunits (trimer and tetramer, respectively). Even if expression levels had been equivalent, other factors, such as the number of HRP molecules appended per ion channel, as well as the exposure of the BBS-tagged site above the plasma membrane, created difficulties in quantitative interpretation. For example, we found that despite having similar expression levels at the plasma membrane(3), the PIEZO1-BBS (cap) construct consistently produced higher signal for the same set of proteins than the PIEZO1-BBS (blade) construct, presumably because the cap domain protrudes higher into extracellular space and is more accessible to labeling(3). In light of these unanticipated challenges, we ultimately chose to generate a stable cell line containing the PIEZO1-BBS (cap) construct and use previous overexpression TMT datasets that we generated during method development as one of our data filters. That is, only proteins captured in the stable cell line dataset (closer to endogenous conditions) and all three complementary overexpression TMT datasets were considered to be potential PIEZO1 interaction partners (see ‘Data analysis’ in the mass spectrometry section of ‘Materials and Methods’). As such, this technique is most amenable to comparisons of the same protein interactome across conditions, such as the presence and absence of a mechanical stimulus. This allows for quantitative analysis of stimulus-specific interactome changes while circumventing the need for other plasma membrane controls that may be more difficult to interpret.

Mass spectrometry (detailed protocol). *Protein precipitation:* Cell pellets collected as described in “proximity labeling” were lysed by probe sonication (10 pulses at 4 °C, 40%, output 4) in 500 µL of ice cold DPBS (Gibco, Cat#14190-136) containing one protease inhibitor cocktail tablet (Roche, cComplete ULTRA tablets, Mini, EDTA-free, Cat#5892791001) per 10 mL. Protein concentrations were quantified using a DC absorbance assay (BioRAD Cat#5000112) and diluted to a final concentration of 3 mg/mL in 500 µL DPBS (1.5 mg of total protein from each 15-cm plate of HEK293T cells). Protein was precipitated by sequential addition and mixing of ice-cold methanol (2 mL), chloroform (0.5 mL), and DPBS (1 mL) followed by vortexing for 30 seconds and centrifugation at 5,000 rpm for 10 minutes to create a protein disk. The top and bottom layers around the disk were gently removed, and the pellet was washed with 2×10 mL of ice-cold methanol with 5,000 rpm centrifugation between washes. After the final wash, the supernatant was carefully removed from the pellet by pipette with a gel-loading tip, and the pellet was allowed to air dry for 15 minutes before further processing. Sample pellets may be stably stored in a –80 °C freezer prior to subsequent denaturing, reducing, and alkylation steps.

Denaturation, reduction, and alkylation: Each protein sample pellet was denatured by adding 500 µL of freshly prepared 6 M urea in DPBS, followed by 10 µL of 10% w/v sodium dodecyl sulfate (SDS) in DPBS. To reduce the protein sample, a solution containing equal volumes of freshly prepared 200 mM tris(2-carboxyethyl)phosphine hydrochloride (TCEP) in DPBS and 600 mM potassium carbonate in DPBS was prepared, and 50 µL of this mixture was added to the denatured sample. Each sample was then probe-sonicated 15× (40%, output 4) and placed in a 37 °C shaker for 30 minutes. Following this incubation, each sample was alkylated by adding 70 µL of 400 mM iodoacetamide in DPBS, briefly mixing, and incubating in the dark at room

temperature for 30 minutes. After alkylation, an additional 130 μ L of 10% SDS in DPBS was added to each sample, then diluted with 5.5 mL of DPBS for a final volume of 6.26 mL per sample (~0.5 M urea, 0.2% w/v SDS).

Streptavidin pull-down and tryptic digest: Streptavidin agarose beads (100 μ L per sample, Thermo Scientific, Cat#20353) were washed 3 \times 500 μ L with DPBS and pelleted at 2000 \times g in between washes. After the final wash, the beads were re-suspended in 100 μ L of DPBS and added to each 6.26-mL protein sample in a 14-mL centrifuge tube. Samples were rotated for 1 h at room temperature on a benchtop end-over-end rotator to pull down biotinylated proteins, followed by pelleting the beads at 2500 \times g for 2 minutes. Supernatant was carefully removed, and the bead slurry was washed sequentially with: 1) 1 \times 5 mL of 0.2% w/v SDS in DPBS, 2) 3 \times 5 mL of DPBS, 3) 1 \times 5 mL of HPLC-grade water, and 4) 2 \times 5 mL of 200 mM EPPS buffer (pH 8.0 with NaOH). Samples were centrifuged at 2500 \times g for 2 minutes in between washes. Beads were resuspended in 500 μ L of EPPS (pH 8.0) and transferred to a 1.5-mL safe-lock, LoBind Eppendorf™ tube (Fisher Scientific, Cat#13-698-794). Residual beads were transferred with an additional 500 μ L of EPPS (total volume of 1 mL) and pelleted at 2500 \times g for 2 minutes. Supernatant was carefully removed from the beads with a fine gel-loading pipette tip. A 20- μ g vial of sequencing-grade trypsin (Promega, Cat# V5111) was dissolved in 2.05 mL of 2 M urea in 200 mM EPPS buffer (pH 8.0). Calcium chloride (100 mM in 200 mM EPPS buffer, pH 8.0) was diluted 1:100 into the trypsin-containing solution (20.5 μ L added, 1 mM final concentration) and gently mixed by pipetting. On-bead tryptic digest was performed by adding 200 μ L of this trypsin solution to each protein sample and incubating for ~14 h on a 37 °C shaker.

TMT labeling and fractionation of peptides: Beads were removed from tryptic peptides by filtering the digested sample through a micro-Bio-Spin chromatography column (Bio-Rad, Cat#7326204) into a clean 2-mL centrifuge tube. HPLC-grade acetonitrile (60 μ L) was added to the eluted peptides (260 μ L total volume), followed by 6 μ L/channel of 10-plex isobaric TMT tag (Thermo Scientific, Cat#90110) dissolved in dry acetonitrile (20 μ g/ μ L). The reaction was allowed to proceed for 1 h at room temperature with an occasional vortex, then quenched with 6 μ L of 5 wt. % hydroxylamine in HPLC-grade water for 15 minutes at room temperature. Formic acid (4 μ L) was added to each sample. All ten TMT-labeled samples were then combined into a single 14-mL centrifuge tube, then divided evenly into four protein LoBind microcentrifuge tubes to dry in a SpeedVac concentrator overnight. The resulting peptide/urea pellets were re-dissolved in Buffer A (95% H₂O, 5% acetonitrile, 0.1% formic acid) and sonicated in a water-bath sonicator for 10 minutes to ensure complete solubilization. Samples were recombined into a single tube followed by addition of 20–60 μ L of HPLC-grade formic acid to reach a pH of 1–3. The peptide sample was manually fractionated offline into 9 fractions on a Pierce™ high pH reversed-phase peptide fractionation column (Thermo Scientific Cat#84868), using a gradient elution of acetonitrile (5, 7.5, 12.5, 15, 20, 25, 30, 40, 50, 80%) in 10 mM aqueous ammonium bicarbonate. Every third fraction (e.g., 1, 4, and 7) of eluted peptides was recombined into a 1.5-mL LoBind Eppendorf tube for a total of 3 fractions and dried overnight in a SpeedVac. Samples were resuspended in buffer A by bath sonication and analyzed on an Orbitrap Fusion mass spectrometer (Thermo Scientific). Data acquisition was by an MS3-based TMT method as previously described(5).

Data analysis: The Integrated Proteomics Pipeline (IP2) was used for initial analysis of raw data files. MS2 and MS3 spectra were analyzed using the ProLucid search algorithm against a non-redundant variant of the human Uniprot database (release-2012_11). Allowed residue modifications in the search algorithm were as follows: static modification of cysteine residues for carboxyamidomethylation (+57.02146 Da), static modification of lysine residues and the N-terminus corresponding to a TMT tag (+229.162932 Da), and differential modification of methionine residues accounting for oxidation (+15.9949 Da). Proteins were required to have at least two peptides for identification with a false discovery rate set at 0.01 and a spectral count (SC) cutoff of 5. Biological replicates of comparison groups were run in duplicate or triplicate for internal TMT comparison and were also repeated in separate TMT runs to ensure reproducibility of results. Four TMT datasets were included in analysis: three with transient overexpression of PIEZO1-BBS (cap) in HEK293T cells and one in the PIEZO1-BBS (cap) stable HEK293F cell line. Proteins not contained in all four TMT datasets were removed from the final list of proteins in the PIEZO1 interactome. Proteins were further ranked by comparing each dataset to the Contaminant Repository for Affinity Purification (CRAPome 2.0), giving priority to proteins found in \leq 25% (179/716) of datasets and thereby

removing contaminants and other highly abundant proteins commonly found in proximity-dependent biotinylation datasets (also see Supplementary File 2). Gene ontology (GO) analysis and manual annotation of the removed proteins based on the Human Protein Atlas(6) showed that the majority of these are annotated as intracellular or cytosolic, likely captured from dead cell debris (Supplementary File 2). To evaluate the extent of background labeling, all datasets were cross-referenced to TMT channels in which all labeling and biotinylation reagents were added to cells expressing mPIEZO1-GFP without a BBS epitope tag. Any proteins equally enriched by PIEZO1 lacking a BBS tag were removed from consideration and included only a small set of biotin-associated proteins (PC, ACACA, ACACB, MCCC1, PCCA) and keratin (KRT), which had previously been eliminated from the datasets by our CRAPome filter.

Calcium imaging additional information. Calcium Ringer's solution used for washing, loading, and imaging cells contained 127 mM NaCl, 3 mM KCl, 10 mM HEPES, 2.5 mM CaCl₂, 1 mM MgCl₂, and 10 mM D-(+)-glucose (pH 7.3 with NaOH, 300-310 mOsm/kg adjusted with D-mannitol). Cells were loaded at room temperature in the dark for 35–40 minutes with ~1 μM Fura2-AM (Life Technologies, Cat#F1201, from a 1 mg/mL stock in DMSO) and 0.02% w/v Pluronic F-127 (Invitrogen, Cat#P6867, from a 20% w/v stock in DMSO freshly prepared and used within one week) in calcium Ringer's. To remove excess dye, cells were washed 3× with calcium Ringer's solution and allowed to sit in the dark for 20 minutes prior to imaging. Yoda1 (TOCRIS, Cat.#558610, CAS#448947-81-7) was prepared as a 2 mM solution in DMSO, diluted 1:200 in calcium Ringer's (10 μM, 2×), and vigorously vortexed 1–2 minutes before adding to each well (final concentration in the well, 5 μM; 170 μL of a 2× solution added to 170 μL of calcium Ringer's in the well). Use of higher stock concentration of Yoda1 and/or preparing the solution ahead of the experiment may result in inconsistent results due to the propensity of Yoda1 to precipitate in aqueous solution over a short time frame. Following 30 seconds of baseline recording, Yoda1 solution was pipetted in a single addition near the bottom corner of the imaging well (without pipetting up and down) to mix with the solution in the chamber as rapidly as possible (peak Yoda1 response occurs within 30 s of addition). Adding a DMSO vehicle control in this manner produced no response, indicating that shear stress was not responsible for the observed effects. At the end of each recording, a 170 μL of a 12 μM (3×) solution of ionomycin calcium salt in calcium Ringer's (Sigma-Aldrich, Cat#I0634 from a 5 mM stock in DMSO) was added to the well (4 μM final concentration in the well). Cells that did not respond to ionomycin were excluded from analysis. Data were acquired every 3 s using MetaFluor (v.7.8.2.0) as a ratio of 340/380nm. At least two wells per gene were tested on the same day. Candidate genes showing consistent effects for both replicates were repeated on at least one other day to confirm the observed effect and then were validated by electrophysiology under the same conditions.

Electrophysiology additional information. Equipment and software. Electrodes (Sutter, Cat#BF150-86-10) were pulled with a Sutter Instruments flaming/brown micropipette puller (Model P-97) and fire polished with a Micro forge (Model MF-830, Narishige, Japan) to a range of resistances from 2–6 MΩ. For poking experiments, the polished glass poke probe was advanced with a ramp speed of 1 μm/ms and held at the indicated position for 125 ms, driven by a piezoelectric controller and actuator (Physik Instrumente, E-625.SR Compact LVPZT controller/amplifier and P-601.1SL PiezoMove® nanopositioning actuator) attached to the micromanipulator with a custom dye-anodized aluminum adapter at an 80° angle to the cell being recorded(7). All recordings were performed using an Axopatch 200B or a Multiclamp 700A amplifier and acquired using Axon™ pClamp10 (Molecular Devices). Data were analyzed using Clampfit 10.6, OriginPro 10 (OriginLab), and GraphPad Prism v.10.1.2 (DotMatics).

Whole-cell recording solutions. Extracellular recording solution contained: 135 mM NaCl, 3 mM KCl, 1 mM MgCl₂, 2.5 mM CaCl₂, 10 mM D-glucose, 10 mM HEPES (pH 7.3 with NaOH; 300-310 mOsm/kg adjusted with D-mannitol to be ~10 mOsm higher than intracellular solution, if necessary). Intracellular recording solution contained: 133 mM CsCl, 5 mM EGTA, 1 mM MgCl₂, 1 mM CaCl₂, 10 mM HEPES, 4 mM Mg·ATP*, 0.4 mM Na₂GTP* (pH 7.3 with CsOH; *10 μL of frozen aqueous ATP and GTP stocks, 400 and 40 mM, respectively, were added to 980 μL aliquots of intracellular solution directly before the experiment, and the pH readjusted back up to 7.3 with ~1.5 μL of 2N CsOH; 285–300 mOsm/kg).

Cell-attached recording solutions and additional details. Extracellular bath solution contained: 140 mM KCl, 1 mM MgCl₂, 10 mM D-glucose, 10 mM HEPES (pH 7.3 with KOH). Pipette solution contained: 130 mM NaCl, 5 mM KCl, 1 mM MgCl₂, 1 mM CaCl₂, 10 mM TEA-Cl, 10 mM HEPES (pH 7.3 with NaOH). Cells were maintained in high-K⁺ bath solution for no longer than 30 minutes. The holding potential was set as -80 mV during recording. Cells were mechanically stimulated as previously described(7) using a high-speed pressure clamp (HSPC-1) device (ALA Scientific Instruments) controlled by Clampex 10.1. A positive pressure pre-pulse of +5 mmHg (5.75 s) was applied followed by a 25-ms step to 0 mmHg before each successive negative pressure step in increments of -5 mmHg. This pre-pulse protocol was shown to minimize membrane curvature and produce maximal response to negative pressure(8).

CADM1 knockdown and overexpression experiments in Neuro-2a cells. *qRT-PCR:* For quantification of siRNA knockdown, RNA was extracted using an RNeasy Micro kit (Qiagen, Cat#74004), according to the manufacturer instructions. The RNeasy kit on-column DNaseI digest step was omitted, and digestion with DNaseI was instead performed immediately prior to reverse transcription, using the Maxima H-minus First Strand cDNA Synthesis Kit with dsDNase (Life Technologies, Cat#K1681). Integrity and purity of input RNA was evaluated by 260/280 nm absorbance ratios (~2). Synthesis of cDNA was performed immediately after RNA isolation, using 1 µg of total RNA and Oligo(dT)₁₈ primers provided in the kit. The cDNA products were diluted 1:25 in nuclease-free water and mixed 1:5 with SyGreen Blue Mix (Genesee Scientific, Cat#16-507) containing the following primer pairs (500 nM):

Gene (amplicon length)	Source	Cat#	Accession#	Primer pairs (5' to 3')
Actb (138 bp)	Origene	MP200232	NM_007393	FWD: CATTGCTGACAGGTGCAGAAGG REV: TGCTGGAAGGTGGACAGTGAGG
Cadm1 (113 bp)	Origene	MP202240	NM_207675	FWD: ACTTCTGCCAGCTCACACGGA REV: CCCTTCAACTGCCGTGTTTC
Cadm1 (99 bp)	Harvard Primer Bank(9–11)	N/A	NM_207675	FWD: CCACAGGTGATGGACAGAAC REV: CTGAGTCGTCACTCTATTGACC

The cycling parameters used for qRT-PCR on a BioRad CFX384 real-time PCR system were 95 °C for 3 minutes and then 40 cycles of 95 °C for 10s and 60 °C for 30s, followed by a melt curve. Primer specificity was evidenced by a single peak in the derivative of the melt curve and by presence of a single band of the expected amplicon length on a 2% agarose gel (Fig. S4, B–C). Differences between the non-targeting scramble control and knockdown conditions were quantified by a change in the C_t value relative to *Actb*, where $\Delta C_t = C_t(\text{Cadm1}) - C_t(\text{Actb})$ for each condition (Fig. S4, D). Fold changes were calculated by the $\Delta\Delta C_t$ method where, $\Delta\Delta C_t = \Delta C_t$ (knockdown condition) – ΔC_t (non-targeting control condition) and fold change = $2^{-(\Delta\Delta C_t)}$ with three biological replicates per condition and three technical replicates per biological replicate.

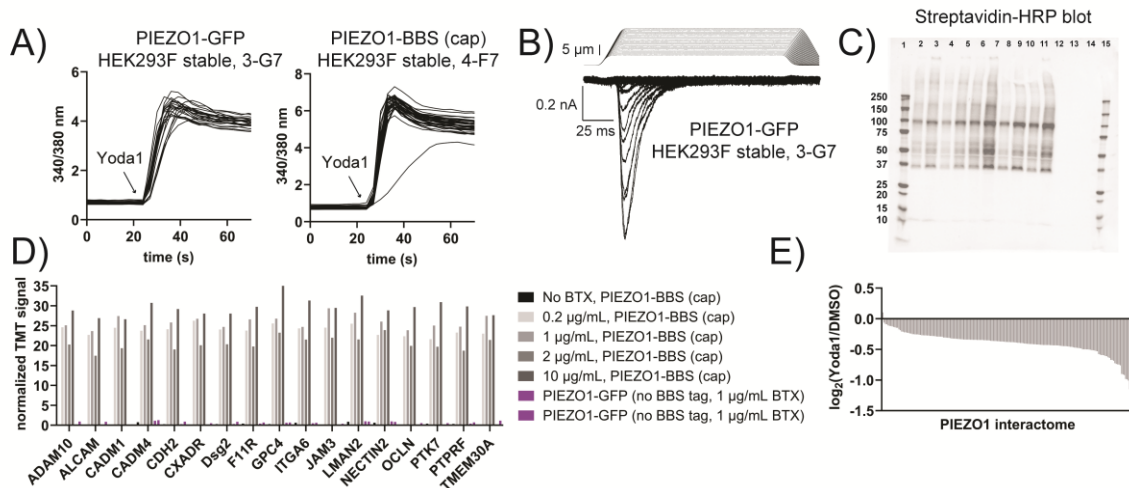


Fig. S1. Functional characterization of PIEZO1 stable cell lines used for proteomics and calcium imaging. A) Representative ratiometric calcium imaging raw data for mPIEZO1-GFP HEK293F stable cells (clone 3-G7) used in the calcium imaging screen and for mPIEZO1-BBS (cap)-GFP HEK293F stable cells (clone 4-F7) used for proximity labeling. Both cell lines produce a fairly uniform increase in intracellular Ca^{2+} in response to 5 μM of the Yoda1 channel agonist. B) Representative family of whole-cell currents elicited in response to poking in increasing 0.5 μm increments to the stable cells (clone 3-G7) used in the calcium imaging screen reveals wild-type-like PIEZO1 kinetics (inactivation tau mean \pm SEM: 9.8 ± 0.7 ms, $n = 24$). C) Representative streptavidin-HRP blot showing the biotinylated proteome of various PIEZO1-BBS (cap) clones derived from the HEK293F stable cell line. In the presence of α -BTX-biotin, H_2O_2 , and biotin-phenol, a range of biotinylated proteins are visible. Clone 4-F7 used for proteomics experiments is shown in lanes 10–11 with 18 or 45 μg of total proteome loaded, respectively. In contrast, no biotinylation is visibly detected for a representative clone derived from the PIEZO1-GFP HEK293F stable cell line in the presence of the same labeling reagents (lanes 12–13). This is consistent with the proteomics data indicating that there is little to no background labeling if the BBS tag is not present (see panel D). D) Representative data from a single TMT optimization experiment in HEK293T cells, showing the relative TMT signal (normalized to 100%) over 7 TMT channels reveals that 0.2 $\mu\text{g}/\text{mL}$ (~ 25 nM) α -BTX performs equivalently to higher concentrations (up to 10 $\mu\text{g}/\text{mL}$, 1.25 μM). Increasing concentrations are shown left to right (gray bars) for a representative set of candidate proteins that were later tested by electrophysiology. Notably, little to no MS signal is detected when cells expressing PIEZO1-BBS (cap) are not exposed to α -BTX prior to biotinylation with H_2O_2 and biotin-phenol (black bars), or when cells expressing PIEZO1-GFP without the BBS tag are exposed to all labeling reagents (fuchsia bars). E) Plot showing the 185 high-confidence PIEZO1 interactome proteins (listed in Figure 1B) in the presence of Yoda1 (10 μM , applied over ~ 1 –2 min.) versus a DMSO vehicle control, averaged over three internal biological replicates in a TMT 6-plex experiment. Experiments were performed with the PIEZO1-BBS (cap) HEK293F stable cell line (clone 4-F7). We observed a small but noticeable and consistent global decrease in the extent of biotinylation in the presence of Yoda1 (see Supporting Information, File 2).

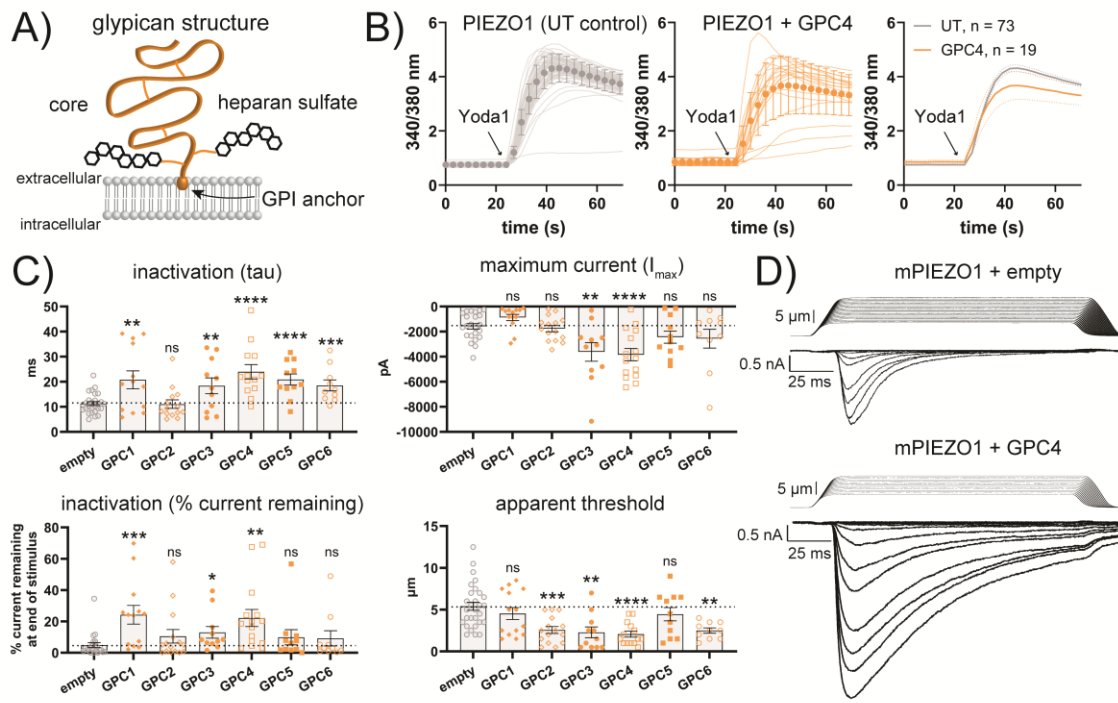


Fig. S2. Characterizing the functional effects of glypcans on PIEZO1. A) Cartoon of glycan (GPC) structure. B) Representative calcium imaging raw data in 3-G7 cells showing the Yoda1 response in cells visibly transfected with GPC4 (orange) vs. untransfected (UT) cells (gray) in the same field of view (n = 19 and n = 73 cells, respectively). Markers show the average \pm SD; Right: average of raw traces shown at the left with dotted lines indicating the 90% confidence interval. C) Whole-cell poke electrophysiology parameters in HEK293T PIEZO1 KO cells co-transfected with mouse *Piezo1*-IRES-GFP and each untagged GPC family member in an IRES-tdTomato vector (see Table S2 for average values and statistical analysis). D) Representative mPIEZO1 whole-cell mechano-currents for PIEZO1 co-expressed with an empty vector control or with GPC4. When overexpressed with GPC4, PIEZO1 expressing cells appeared sensitized to mechanical indentation (i.e., they exhibited a lower apparent threshold), had larger apparent maximal currents, and inactivated more slowly than wild-type mPIEZO1. In the mPIEZO1 + GPC4 example shown, PIEZO1 began responding at a shallow indentation depth of 1 μ m and reached its maximum current before the top wild-type mPIEZO1 cell started responding (5.5 μ m).

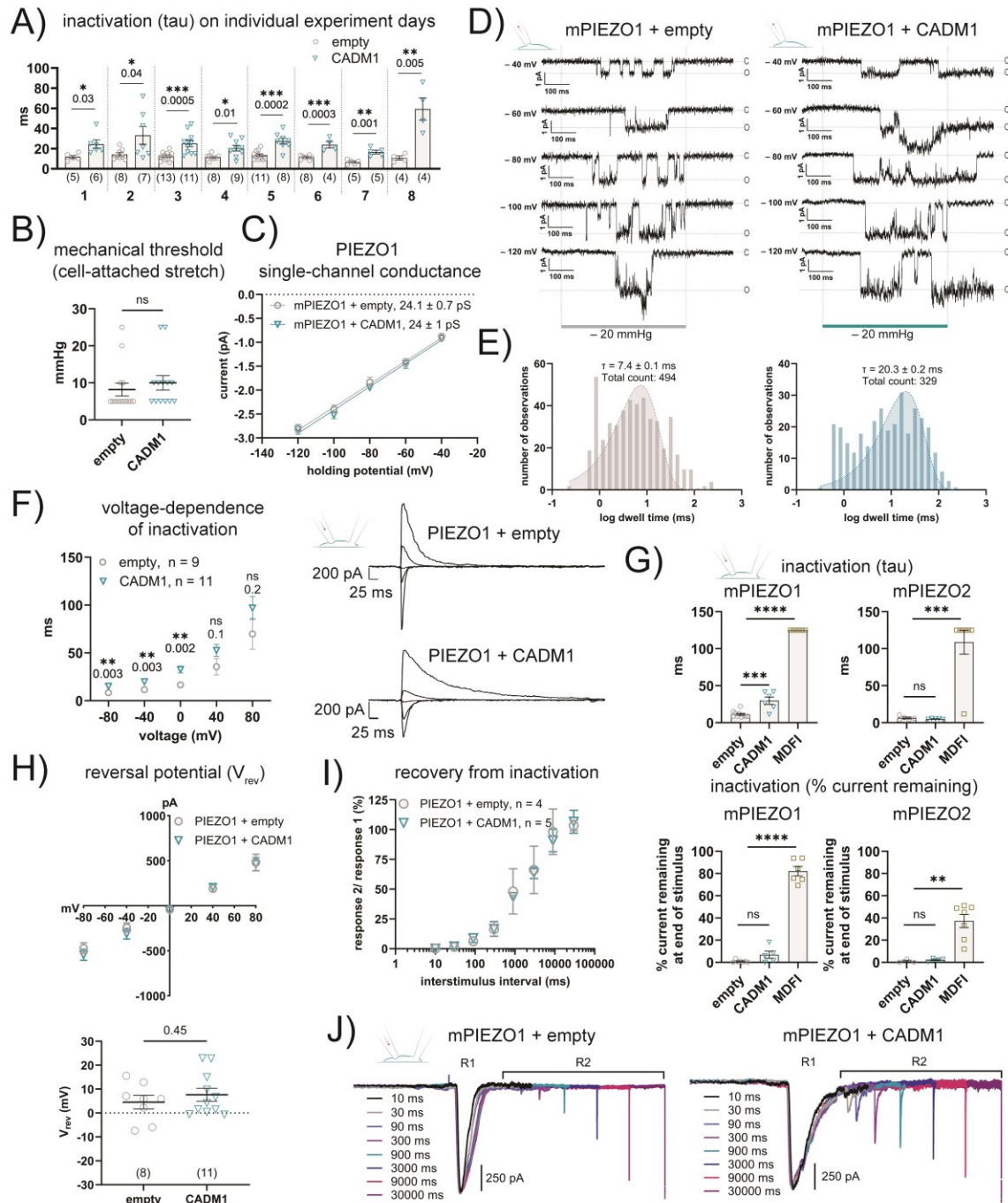


Fig. S3. Additional characterization of CADM1 on PIEZO1 and PIEZO2. All values in this figure are expressed as the mean \pm SEM. A) Inactivation time constant (τ , ms) of whole-cell poking-induced mPIEZO1 currents in cells transfected with mouse *Piezo1* and either an empty vector control or co-expressed with *CADM1* on individual recording days (1–8) in HEK293T PIEZO1 knockout cells, shown as pooled data in Figure 3A. The number of cells for each condition (n) are indicated below each bar, and the p -values, as calculated by an unpaired two-tailed t -test, are shown on the graph. B) Quantification of the PIEZO1 mechanical threshold in cell-attached stretch assay in HEK293T PIEZO1 knockout cells overexpressing an empty vector or CADM1 (empty: 8 ± 2 mmHg, $n = 14$; CADM1: 10 ± 2 mmHg, $n = 13$; $p = 0.5$). These results are consistent with little to no change in the mechanical threshold of PIEZO1 with CADM1 in whole-cell poke experiments

(Table S1, Appendix I). C) Summary data of PIEZO1 unitary conductance as measured by recordings in panel D, showing no change in single-channel conductance in the presence of CADM1 (empty: 24.1 ± 0.7 pS, n = 5 vs. CADM1: 24 ± 1 pS, n = 5). D) Representative cell-attached stretch single-channel recordings for PIEZO1 in the presence of overexpressed empty vector control or CADM1. Data are shown for the same cell with voltage steps from -40 to -120 mV in 20 mV increments and an applied negative pressure stimulus of -20 mm Hg for 500 ms (stimulus duration shown by gray/turquoise bar; C = closed, O = open). E) Histograms of open-channel dwell times from single-channel recordings of PIEZO1 in the absence (gray) or presence (turquoise) of CADM1, showing a nearly 3-fold increase in the time PIEZO1 spends open when CADM1 is present (empty: 7.4 ± 0.1 ms, event count = 494; CADM1: 20.3 ± 0.2 ms, event count = 329). F) PIEZO1 voltage-dependence of inactivation as measured by whole-cell poke electrophysiology at -80 , -40 , 0 , $+40$, and $+80$ mV in the presence of an empty vector control or CADM1 overexpressed in HEK293T PIEZO1 KO cells. Representative traces are shown at the right with quantification shown left for the indicated number of cells. Inactivation is slower and more variable at positive voltages and is not statistically significant for this number of cells, but CADM1 appears to slow inactivation at all voltages. G) Comparison of the effects of CADM1 and MDFI on PIEZO1 and PIEZO2 from whole-cell poke recordings performed in parallel on the same day. Co-expression with MDFI showed an inactivating phenotype for both mPIEZO1 and mPIEZO2. For MDFI, tau is plotted at 125 ms, the end of the stimulus, but the current persisted beyond the end of the mechanical indentation (n = 6, $p < 0.0001$ and n = 7, $p = 0.0004$ for PIEZO1 and PIEZO2, respectively), as previously reported(12). This stands in contrast to CADM1, which produced a noticeable effect on inactivation with PIEZO1 (empty tau: 11 ± 1 ms, n = 10; CADM1 tau: 30 ± 5 ms, n = 6; $p = 0.0007$) but not PIEZO2 (empty tau: 6 ± 1 ms, n = 5; CADM1 tau: 5.1 ± 0.3 ms, n = 5; $p = 0.3$). In the presence of MDFI, PIEZO2 inactivated to a greater extent than PIEZO1 over this 125-ms interval but was still significantly inactivating in both conditions (as measured by the percent current remaining at the end of the stimulus). CADM1 showed a trend towards more current remaining at the end of the stimulus, in line with the results in Fig. 3A (current remaining: PIEZO1 + empty, $0.9 \pm 0.5\%$, n = 7; PIEZO1 + CADM1, $7 \pm 3\%$, n = 5; PIEZO1 + MDFI, $82 \pm 4\%$, n = 6; empty vs. CADM1, $p = 0.05$; empty vs. MDFI, $p < 0.0001$; PIEZO2 + empty, $1 \pm 1\%$, n = 3; PIEZO2 + CADM1, $2.2 \pm 0.7\%$, n = 3; PIEZO2 + MDFI, $37 \pm 6\%$, n = 7; empty vs. CADM1, $p = 0.3$; empty vs. MDFI, $p = 0.005$). H) Evaluation of the mPIEZO1 reversal potential. Top: Average linear current-voltage (I-V) relationship as measured by whole-cell poke electrophysiology, as in panel F. Reversal potential is the voltage at which the current intercepts the x-axis for mouse *Piezo1* co-transfected with an empty vector (gray) or *CADM1* (turquoise). Bottom: mPIEZO1 reversal potentials for individual cells included in the average shown in the top panel, showing no statistical difference between the empty control and CADM1 (mean \pm SEM, empty: 5 ± 3 mV, n = 8; CADM1: 8 ± 3 mV, n = 11, $p = 0.5$). I) mPIEZO1 recovery from inactivation as measured by whole-cell poke electrophysiology in the presence of empty vector control or CADM1 in HEK293T PIEZO1 KO cells. Cells were subjected to a two-step indentation protocol of 100 ms with an interstimulus interval ranging from 10 ms to 30 s. The magnitude of the second response (R2) was measured as a percentage of the first response (R1) at 8 time intervals, as shown for the representative traces in Panel J. Summary data are shown with R2/R1 shown as a function of the interstimulus interval. Fitting of this function indicates no difference between mPIEZO1 with an empty vector control vs. CADM1 (recovery time constant: PIEZO1 + empty, 1.1 ± 0.2 s, n = 4; PIEZO1 + CADM1, 1.3 ± 0.2 s, n = 5). J) Representative recovery from inactivation traces. The x-axis is shown on a base-10 log scale for visualization of all interstimulus intervals in the same plot for a single cell. R1 values are normalized to a single peak value for easier visualization of the current recovery.

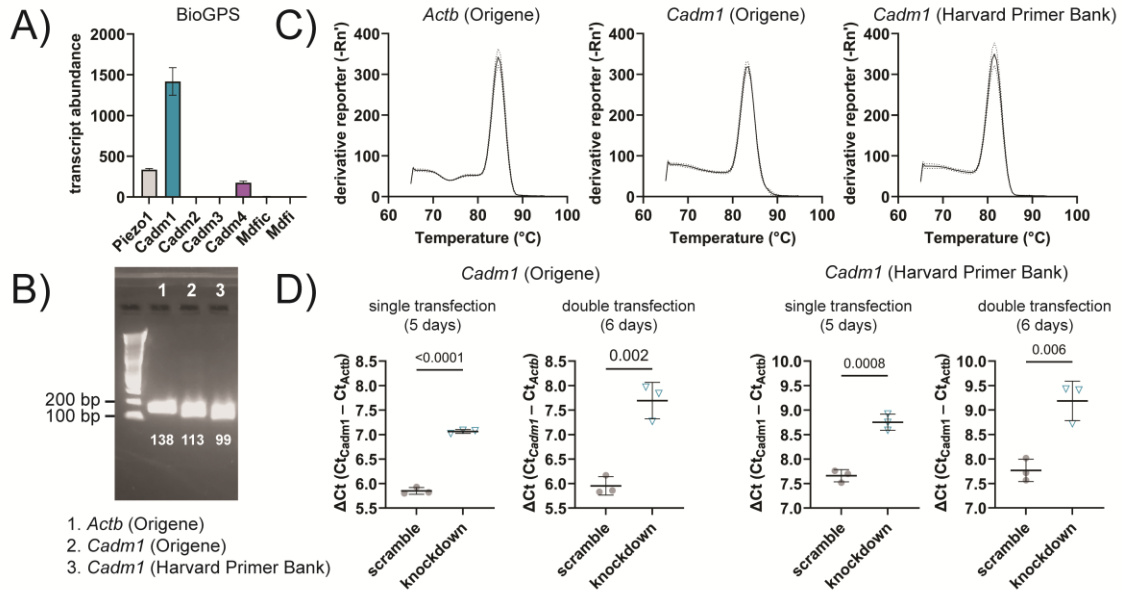


Fig. S4. *Cadm1* knockdown primer validation and qPCR in N2a cells. A) Relative abundance of *Piezo1* transcript compared to *Cadm1–4*, *Mdfic*, and *Mdfi* in N2a cells, as reported in the BioGPS database (mean \pm SD)(13). B) Visualization of DNA amplicons on a 2% agarose gel, showing a single PCR product of the expected length for each of the qPCR primers used in this study. C) Representative derivative melt curves for *Actb* and *Cadm1* primers, showing the mean \pm SD for 3 technical replicates of a single sample. D) Quantification of *Cadm1* siRNA knockdown by two different primer pairs (Origene or Harvard Primer Bank) under two different transfection conditions. Each point on the plot represents the average of three technical replicates for one biological replicate. The mean \pm SD of the ΔCt values for three biological replicates (non-targeting scramble control siRNA or *Cadm1* knockdown condition) are shown in each plot. Significance is shown as a p-value from an unpaired t-test. Similar knockdown efficiencies were obtained by each of the *Cadm1* primer pairs and correspond to \sim 53–57% transcript knockdown 5 days after a single transfection with siRNA or \sim 62–70% transcript knockdown 6 days after two transfections (3 days apart). The double transfection protocol was employed for all electrophysiology experiments in N2a cells. The pooled knockdown efficiency is likely an underestimate of the true knockdown efficiency in single cells, given that not every cell is transfected. Only cells containing a fluorescent transfection marker were included in electrophysiology experiments.

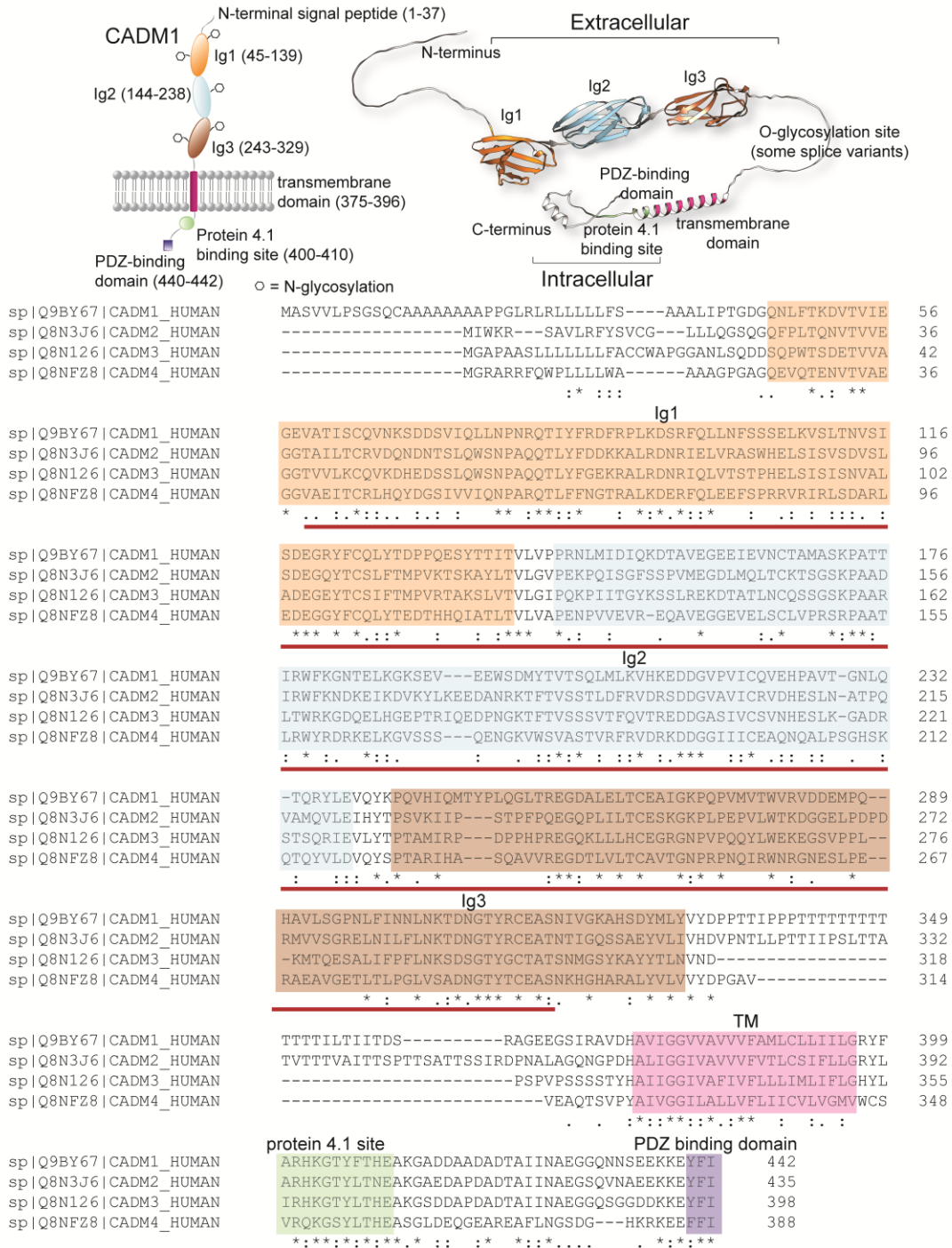


Fig. S5. Sequence conservation across the cell adhesion molecule (CADM) family. Sequence alignments for human CADM1–4 are colored to match the cartoon and protein structure shown at the top. The red lines below the sequence indicate the regions of CADM1 that are absent in the ΔIg/ΔCT mutant.

Table S1. Whole-cell ‘poke’ electrophysiology screen of PIEZO1 interaction candidates. Mean inactivation time constant (τ), inward peak current (I_{max}), apparent mechanical threshold, and percent of peak current remaining at the end of a mechanical poke stimulus \pm SEM at -80 mV, as shown in Fig. 2C and Appendix I. P -values are calculated from an unpaired two-tailed t -test comparing HEK293T PIEZO1 knockout cells transfected with mouse *Piezo1*-IRES-GFP and each candidate gene or an empty control vector containing a fluorescent marker. Each candidate was compared to the empty control vector transfected on the same day as each candidate for comparison, using similar numbers of individual cells ('n') and identical experiment conditions. Candidates showing any statistical trend or significance on a single day of recording were repeated on at least one additional day for confirmation of results. One cell for CADM1 and two cells for GPC4 revealed little inactivation during the stimulus (>125 ms, no exponential could be fit) and were not included in statistical analysis of τ . This was not observed in any of the other conditions and is consistent with the slow inactivation phenotype that we observe for PIEZO1 under these two conditions.

Inactivation time constant (τ)						
candidate gene	τ (ms) empty	τ (ms) candidate	p -value	significance	'n' empty	'n' candidate
ADAM10	13 ± 2	14 ± 3	0.8	ns	10	6
ALCAM	14 ± 1	16 ± 2	0.3	ns	13	10
CADM1	11.9 ± 0.5	27 ± 2	<0.0001	****	62	54
CADM4	14 ± 1	22 ± 4	0.04	*	15	11
CDH2	13 ± 2	12 ± 2	0.7	ns	10	8
CXADR	13 ± 1	16 ± 1	0.02	*	11	14
Dsg2	13 ± 2	11 ± 2	0.5	ns	10	7
F11R	14 ± 1	17 ± 2	0.2	ns	13	13
GPC4	12.5 ± 0.7	20 ± 2	0.0002	***	51	38
ITGA6	12 ± 1	11 ± 1	0.6	ns	19	11
JAM3	13 ± 1	15 ± 2	0.3	ns	15	8
LMAN2	11.6 ± 0.6	16 ± 2	0.07	ns	16	16
NECTIN2	13 ± 1	17 ± 2	0.1	ns	15	7
OCLN	13 ± 1	13 ± 1	0.8	ns	16	12
PTK7	13 ± 2	14 ± 2	0.8	ns	17	6
PTPRF	14 ± 2	16 ± 2	0.4	ns	15	10
TMEM30A	11.2 ± 0.6	10 ± 1	0.2	ns	22	11
Apparent maximal current (I_{max})						
candidate gene	I_{max} (nA) empty	I_{max} (nA) candidate	p -value	significance	'n' empty	'n' candidate
ADAM10	-1.5 ± 0.3	-1.1 ± 0.4	0.5	ns	10	6
ALCAM	-1.1 ± 0.2	-2.5 ± 0.8	0.07	ns	13	10
CADM1	-1.5 ± 0.2	-1.7 ± 0.2	0.5	ns	58	53
CADM4	-0.7 ± 0.1	-0.7 ± 0.2	0.7	ns	11	10
CDH2	-1.5 ± 0.3	-1.7 ± 0.4	0.6	ns	10	7
CXADR	-1.4 ± 0.3	-3.2 ± 0.4	0.003	**	10	14
Dsg2	-1.5 ± 0.3	-1.7 ± 0.3	0.6	ns	10	7
F11R	-1.1 ± 0.2	-2.9 ± 0.6	0.01	**	13	12
GPC4	-1.4 ± 0.1	-3.3 ± 0.3	<0.0001	****	46	39
ITGA6	-2.5 ± 0.6	-1.9 ± 0.4	0.4	ns	16	11
JAM3	-1.3 ± 0.2	-1.8 ± 0.4	0.2	ns	14	7
LMAN2	-1.6 ± 0.4	-1.8 ± 0.3	0.7	ns	16	16
NECTIN2	-1.0 ± 0.2	-1.5 ± 0.6	0.3	ns	13	6
OCLN	-1.3 ± 0.2	-2.7 ± 0.7	0.03	*	14	10

PTK7	-1.3 ± 0.2	-1.0 ± 0.2	0.4	ns	15	6
PTPRF	-1.1 ± 0.2	-1.5 ± 0.2	0.3	ns	14	10
TMEM30A	-1.7 ± 0.3	-1.0 ± 0.2	0.2	ns	20	8

Apparent mechanical threshold (μm of indentation at first response)

candidate gene	threshold (μm) empty	threshold (μm) candidate	p-value	significance	'n' empty	'n' candidate
ADAM10	7 ± 1	8 ± 2	0.6	ns	11	6
ALCAM	10 ± 1	5 ± 1	0.003	**	14	10
CADM1	8.2 ± 0.4	7.0 ± 0.4	0.04	*	65	55
CADM4	8.5 ± 0.9	8 ± 1	0.9	ns	15	12
CDH2	7 ± 1	8 ± 1	0.4	ns	11	8
CXADR	9.5 ± 0.9	8 ± 1	0.2	ns	13	14
Dsg2	7 ± 1	6.5 ± 0.5	0.7	ns	11	7
F11R	10 ± 1	8 ± 1	0.1	ns	14	13
GPC4	6.7 ± 0.4	4.0 ± 0.4	<0.0001	****	53	40
ITGA6	9 ± 1	8.2 ± 0.8	0.4	ns	20	12
JAM3	11 ± 1	8 ± 2	0.1	ns	17	8
LMAN2	8.2 ± 0.8	8.1 ± 0.8	0.9	ns	16	19
NECTIN2	10 ± 1	9 ± 1	0.4	ns	16	8
OCLN	8.6 ± 0.9	10 ± 1	0.5	ns	16	13
PTK7	10 ± 1	8 ± 2	0.3	ns	18	7
PTPRF	8.5 ± 0.7	10 ± 1	0.4	ns	15	13
TMEM30A	9.4 ± 0.8	10 ± 1	0.9	ns	23	13

Percent of maximal current (I_{max}) remaining at the end of the stimulus

candidate gene	% of I_{max} empty	% of I_{max} candidate	p-value	significance	'n' empty	'n' candidate
ADAM10	6 ± 4	18 ± 15	0.4	ns	10	6
ALCAM	4 ± 2	4 ± 2	0.8	ns	13	10
CADM1	2.8 ± 0.7	11 ± 2	0.0004	***	58	53
CADM4	6 ± 3	10 ± 5	0.4	ns	11	9
CDH2	6 ± 3	0.7 ± 0.3	0.2	ns	10	7
CXADR	2 ± 1	8 ± 5	0.3	ns	10	14
Dsg2	7 ± 4	3 ± 1	0.4	ns	10	7
F11R	4 ± 2	8 ± 6	0.4	ns	13	12
GPC4	4 ± 1	11 ± 3	0.01	*	46	39
ITGA6	6 ± 3	4 ± 1	0.7	ns	16	11
JAM3	3 ± 2	3 ± 1	1	ns	14	7
LMAN2	5 ± 2	3 ± 1	0.5	ns	16	16
NECTIN2	5 ± 2	2 ± 1	0.4	ns	13	6
OCLN	3 ± 1	2.2 ± 0.8	0.7	ns	14	10
PTK7	3 ± 1	8 ± 3	0.07	ns	15	6
PTPRF	3 ± 1	3.0 ± 0.6	0.8	ns	14	10
TMEM30A	4 ± 2	3 ± 1	0.7	ns	20	8

Table S2. Whole-cell ‘poke’ electrophysiology summary of glypcan overexpression with mPIEZ01. Mean inactivation time constant (τ), peak current (I_{max}), apparent mechanical threshold, and percent of peak current remaining at the end of a mechanical poke stimulus \pm SEM at -80 mV, as shown in Fig. S2. P -values are calculated from an unpaired two-tailed t -test comparing HEK293T PIEZ01 KO cells transfected with *Piezo1*-IRES-GFP and each GPC or an empty control vector containing a fluorescent marker. Experiments were performed with 4 independent transfections on 4 separate days. Each GPC was compared to the empty control vector transfected on the same day as each candidate for comparison, using similar numbers of individual cells ('n') and identical experiment conditions. Two cells for GPC4 revealed little inactivation during the stimulus (>125 ms, no exponential could be fit) and were not included in the statistical analysis of τ . This was not observed in any of the other conditions.

Inactivation time constant (τ)						
candidate gene	τ (ms) empty	τ (ms) candidate	p -value	significance	'n' empty	'n' candidate
GPC1	11.3 ± 0.8	21 ± 4	0.001	**	27	13
GPC2	11.3 ± 0.8	11 ± 2	0.9	ns	27	14
GPC3	11.3 ± 0.8	18 ± 3	0.004	**	27	11
GPC4	11.3 ± 0.8	24 ± 3	<0.0001	****	27	13
GPC5	11.3 ± 0.8	21 ± 2	<0.0001	****	27	11
GPC6	11.3 ± 0.8	19 ± 2	0.0003	***	27	10
Apparent maximal current (I_{max})						
candidate gene	I_{max} (nA) empty	I_{max} (nA) candidate	p -value	significance	'n' empty	'n' candidate
GPC1	-1.6 ± 0.2	-0.9 ± 0.3	0.05	ns	23	13
GPC2	-1.6 ± 0.2	-1.8 ± 0.3	0.6	ns	23	15
GPC3	-1.6 ± 0.2	-3.6 ± 0.7	0.002	**	23	11
GPC4	-1.6 ± 0.2	-3.8 ± 0.5	<0.0001	****	23	15
GPC5	-1.6 ± 0.2	-2.4 ± 0.5	0.07	ns	23	11
GPC6	-1.6 ± 0.2	-2.6 ± 0.8	0.1	ns	23	10
Apparent mechanical threshold (μm of indentation at first response)						
candidate gene	threshold (μm) empty	threshold (μm) candidate	p -value	significance	'n' empty	'n' candidate
GPC1	5.4 ± 0.5	4.5 ± 0.7	0.3	ns	29	14
GPC2	5.4 ± 0.5	2.6 ± 0.4	0.0004	***	29	15
GPC3	5.4 ± 0.5	2.3 ± 0.6	0.001	**	29	11
GPC4	5.4 ± 0.5	2.1 ± 0.4	<0.0001	****	29	14
GPC5	5.4 ± 0.5	4.5 ± 0.8	0.3	ns	29	11
GPC6	5.4 ± 0.5	2.5 ± 0.3	0.002	**	29	10
Percent of maximal current (I_{max}) remaining at the end of the stimulus						
candidate gene	% of I_{max} empty	% of I_{max} candidate	p -value	significance	'n' empty	'n' candidate
GPC1	5 ± 2	24 ± 6	0.0005	***	22	13
GPC2	5 ± 2	11 ± 4	0.2	ns	22	15
GPC3	5 ± 2	13 ± 4	0.02	*	22	11
GPC4	5 ± 2	22 ± 5	0.001	**	22	15
GPC5	5 ± 2	10 ± 5	0.2	ns	22	11
GPC6	5 ± 2	9 ± 5	0.3	ns	22	10

Table S3. Effect of CADM1 on mPIEZO2. Whole-cell poke electrophysiology data are shown as mean \pm SEM at -80 mV. *P*-values are calculated from an unpaired two-tailed *t*-test comparing HEK293T PIEZO1 knockout cells transfected with mouse *Piezo2*-IRES-mNeonGreen and CADM1 (wild-type) or an empty control vector containing a fluorescent marker. Each candidate was compared to the empty control vector transfected on the same day as each candidate for comparison, using similar numbers of individual cells ('n') and identical experiment conditions. Statistical analysis represents pooled data from 4 independent transfections (4 separate recording days).

'poke' parameter	PIEZO2 + empty control	PIEZO2 + CADM1	p-value	significance	'n' empty	'n' CADM1
$\tau_{\text{inactivation}}$ (ms)	5.7 ± 0.4	6.1 ± 0.5	0.6	ns	25	22
I_{\max} (nA)	-0.8 ± 0.1	-0.9 ± 0.1	0.6	ns	23	19
threshold (μm)	6.9 ± 0.6	6.9 ± 0.6	1	ns	19	16
remaining current (% of I_{\max})	1.1 ± 0.3	2.5 ± 0.5	0.02	*	23	19

Table S4. Effect of CADM1 overexpression on endogenous mPIEZO1 in N2a cells. Whole-cell poking electrophysiology data are shown as mean \pm SEM at -80 mV. *P*-values are calculated from an unpaired two-tailed *t*-test comparing endogenous mPIEZO1 currents in cells transfected with *CADM1*-IRES-tdTomato or with those expressing an empty control vector containing a fluorescent marker. CADM1-expressing cells were compared to the empty control vector transfected on the same day, using similar numbers of individual cells ('n') and identical experiment conditions. Statistical analysis represents pooled data from 3 independent transfections/recording days.

'poke' parameter	PIEZO1 + empty control	PIEZO1 + CADM1	p-value	significance	'n' empty	'n' CADM1
$\tau_{\text{inactivation}}$ (ms)	12.2 ± 0.8	22 ± 2	0.0006	***	14	17
I_{\max} (nA)	-0.2 ± 0.05	-0.2 ± 0.02	0.6	ns	15	17
threshold (μm)	2.4 ± 0.5	3.7 ± 0.5	0.09	ns	15	17
remaining current (% of I_{\max})	1.1 ± 0.9	9 ± 2	0.01	*	14	17

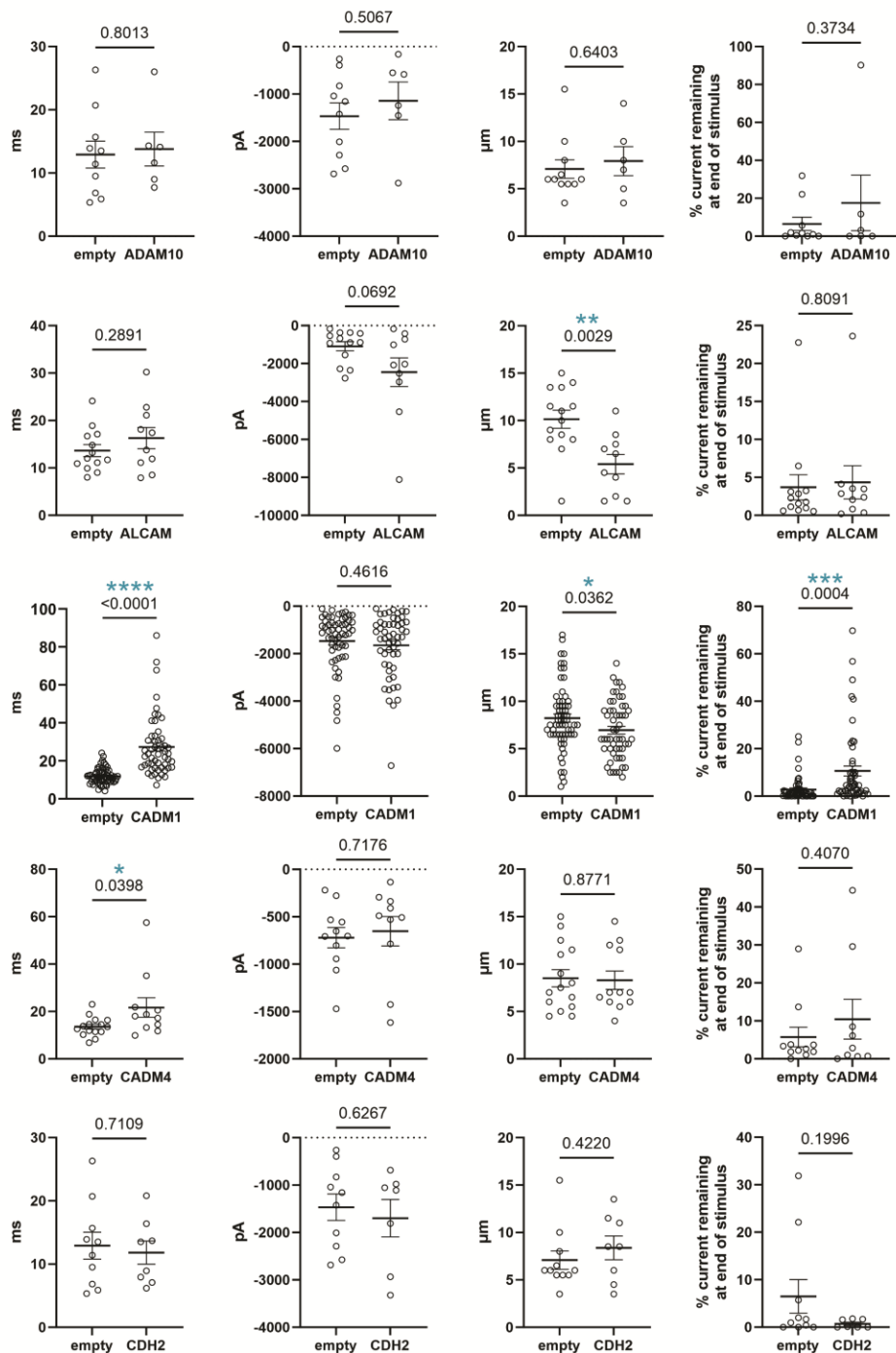
Table S5. Effect of *Cadm1* knockdown on endogenous mPIEZ01 in N2a cells. Whole-cell ‘poke’ electrophysiology data are shown as mean \pm SEM at -80 mV. *P*-values are calculated from an unpaired two-tailed *t*-test comparing endogenous mPIEZ01 currents in cells transfected with either a non-targeting control RNA or si*Cadm1* and co-transfected with an empty vector containing a fluorescent marker. Statistical analysis represents pooled data from 3 independent transfections (3 separate recording days).

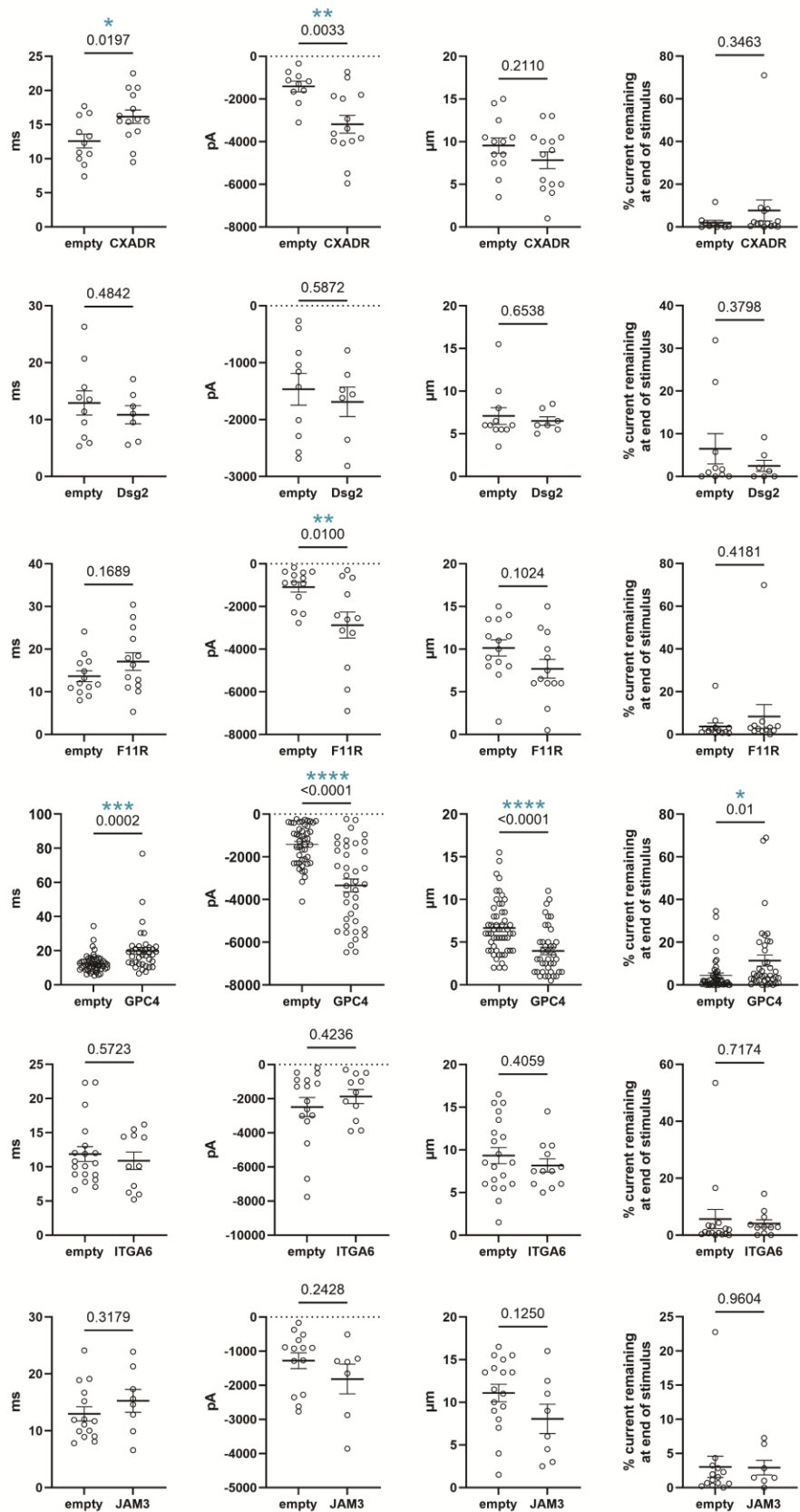
‘poke’ parameter	PIEZ01 + non-targeting control	PIEZ01 + si <i>Cadm1</i>	<i>p</i> -value	significance	‘n’ control	‘n’ si <i>Cadm1</i>
$\tau_{\text{inactivation}}$ (ms)	11.0 ± 0.7	8.8 ± 0.5	0.01	*	34	35
I_{\max} (nA)	-0.26 ± 0.03	-0.26 ± 0.03	0.9	ns	32	30
threshold (μm)	7.3 ± 0.5	7.1 ± 0.4	0.8	ns	46	43
remaining current (% of I_{\max})	2.3 ± 0.7	1.0 ± 0.2	0.1	ns	32	30

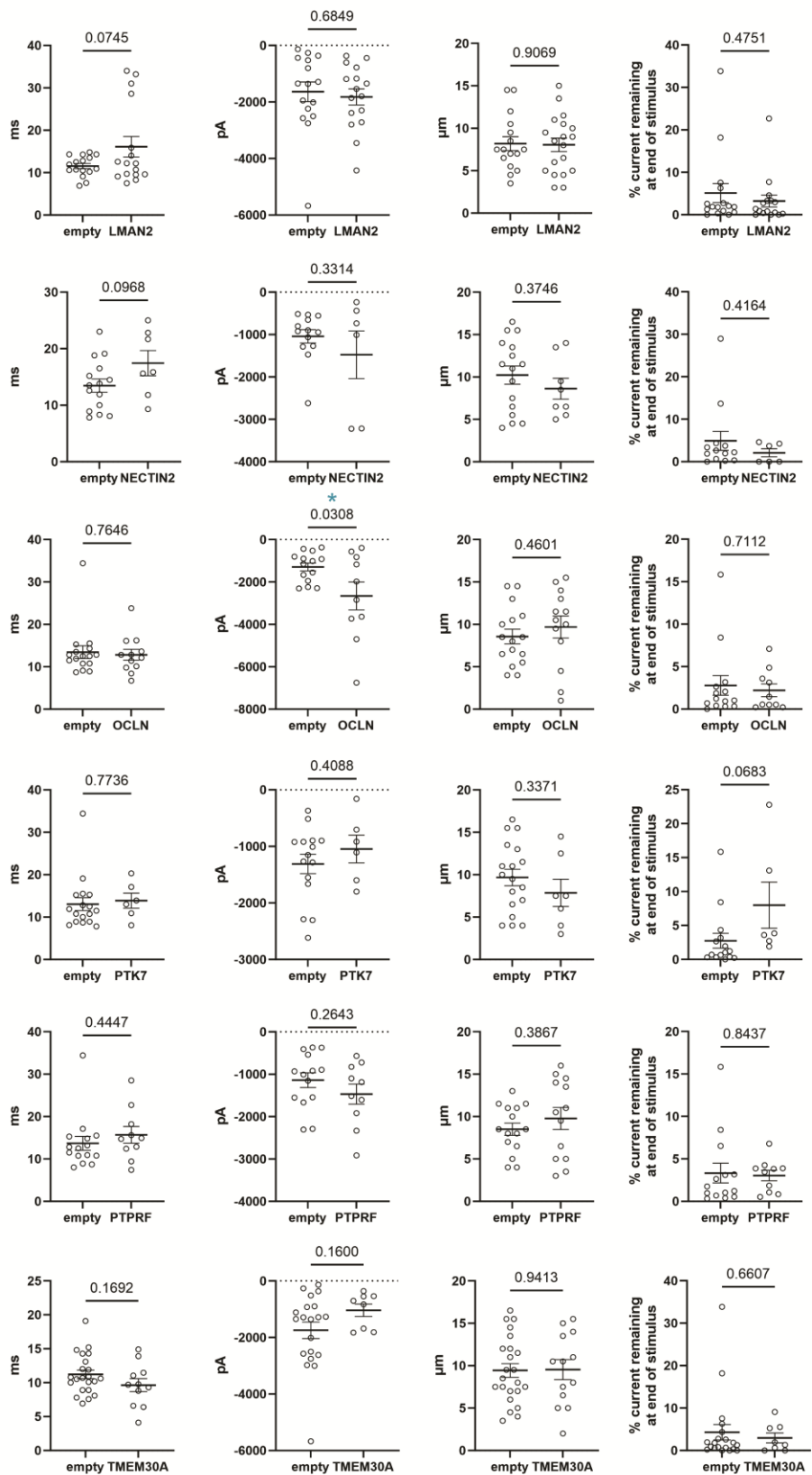
Table S6. Whole-cell ‘poke’ electrophysiology evaluation of CADM1 mutants co-transfected with PIEZO1. Mean inactivation time constant (τ , as shown in Fig. 4B), inward peak current (I_{max}), apparent mechanical threshold, and percent of peak current remaining at the end of a mechanical poke stimulus \pm SEM at -80 mV. P -values are calculated from an unpaired two-tailed t -test comparing HEK293T PIEZO1 knockout cells transfected with mouse *Piezo1*-IRES-GFP and CADM1 (wild-type, WT or mutant) or an empty control vector containing a fluorescent marker. Each candidate was compared to the empty control vector transfected on the same day as each candidate for comparison, using similar numbers of individual cells ('n') and identical experiment conditions. Statistical analysis represents pooled data from 2–4 independent transfections (2–4 separate recording days). Empty control and WT CADM1 were recorded on every experiment day to ensure day-to-day consistency for better comparison to the mutants. The experimenter was blinded to the identity of the conditions until after data analyses were performed. None of the CADM1 mutants were significantly different from wild-type CADM1 (ΔI_g , $p = 0.5$; ΔC T, $p = 0.7$; ΔP DZ, $p = 0.5$; $\Delta I_g/\Delta C$ T, $p = 0.2$).

Inactivation time constant (τ)						
candidate gene	τ (ms) empty	τ (ms) candidate	p -value	significance	'n' empty	'n' candidate
CADM1 (WT)	12.3 ± 0.6	24 ± 2	<0.0001	****	40	32
CADM1 (ΔI_g)	12.0 ± 0.8	21 ± 3	0.0005	***	21	12
CADM1 (ΔCT)	12.0 ± 0.8	24 ± 2	<0.0001	****	21	10
CADM1 (ΔPDZ)	12.0 ± 0.8	21 ± 2	<0.0001	****	21	9
CADM1 ($\Delta I_g/\Delta C$T)	12.6 ± 0.9	23 ± 1	<0.0001	****	19	15
Apparent maximal current (I_{max})						
candidate gene	I_{max} (nA) empty	I_{max} (nA) candidate	p -value	significance	'n' empty	'n' candidate
CADM1 (WT)	-1.6 ± 0.2	-1.6 ± 0.2	0.7	ns	37	31
CADM1 (ΔI_g)	-2.0 ± 0.3	-2.0 ± 0.3	0.9	ns	20	12
CADM1 (ΔCT)	-2.0 ± 0.3	-3.2 ± 0.9	0.1	ns	20	8
CADM1 (ΔPDZ)	-2.0 ± 0.3	-1.6 ± 0.3	0.5	ns	20	9
CADM1 ($\Delta I_g/\Delta C$T)	-1.3 ± 0.3	-2.2 ± 0.5	0.1	ns	17	15
Apparent mechanical threshold (μ m of indentation at first response)						
candidate gene	threshold (μ m) empty	threshold (μ m) candidate	p -value	significance	'n' empty	'n' candidate
CADM1 (WT)	8.0 ± 0.5	7.5 ± 0.6	0.5	ns	40	33
CADM1 (ΔI_g)	7.9 ± 0.5	7 ± 1	0.5	ns	21	13
CADM1 (ΔCT)	7.9 ± 0.5	6.7 ± 0.9	0.2	ns	21	10
CADM1 (ΔPDZ)	7.9 ± 0.5	7.7 ± 0.8	0.8	ns	21	9
CADM1 ($\Delta I_g/\Delta C$T)	8.2 ± 0.9	7.0 ± 0.9	0.4	ns	19	15
Percent of maximal current (I_{max}) remaining at the end of the stimulus						
candidate gene	% of I_{max} empty	% of I_{max} candidate	p -value	significance	'n' empty	'n' candidate
CADM1 (WT)	2.9 ± 0.8	10 ± 3	0.006	**	37	31
CADM1 (ΔI_g)	1.8 ± 0.5	13 ± 5	0.01	*	20	12
CADM1 (ΔCT)	1.8 ± 0.5	12 ± 2	<0.0001	****	20	8
CADM1 (ΔPDZ)	1.8 ± 0.5	10 ± 2	<0.0001	****	20	9
CADM1 ($\Delta I_g/\Delta C$T)	4 ± 2	5 ± 1	0.7	ns	17	15

Appendix I: Electrophysiology screen. Whole-cell poke electrophysiology data of all candidates listed in Table S1, shown alphabetically. Left to right: inactivation time constant (τ), I_{max} , apparent threshold, and % current remaining at the end of the mechanical poking stimulus.







Appendix II: cDNA library information. List of candidate genes used for constructs in this study and their commercial sources. Sequences were subcloned from the commercial vectors into expression vectors via Gateway recombination or PCR-based cloning as described in ‘Materials and Methods’. If the gene did not express, this is indicated in the ‘Notes’ column. If purchased sequences deviate from those reported in UniProt, this has been noted below each protein sequence following the main table. Protein sequences are provided following the main table.

Gene	UniProt ID	cDNA source (company)	cDNA source (cat#)	Backbone(s)	Notes
ADAM10	O14672-1	Addgene	Plasmid #65106	IRES-tdTomato	Gschwind, et al. <i>EMBO J.</i> 2003, 22(10):2411
ALCAM	Q13740-1	Horizon Discovery, hORFeome v8.1	OHS6084-202634686	IRES-tdTomato, C-term mCherry (Addgene Plasmid #31907)	
ANO6	Q4KMQ2-1	Horizon Discovery, hORFeome v8.1	OHS6084-202637663	C-term 2HA (Addgene Plasmid #118374)	<i>no expression</i>
Ano6	Q6P9J9-1	Addgene	Plasmid #62554	C-term mCherry	used as purchased
ATP1B1	P05026-1	Horizon Discovery, hORFeome v8.1	OHS6084-202629350	C-term mCherry (Addgene Plasmid #31907)	
BCAM	P50895	Horizon Discovery, hORFeome v8.1	OHS6084-202630130	C-term mCherry (Addgene Plasmid #31907)	
CADM1	Q9BY67-1	GenScript	gene synthesis	IRES-tdTomato	mammalian codon-optimized
CADM1	A0A4Z1	Horizon Discovery, hORFeome v8.1	OHS6084-202639433	C-term mCherry (Addgene Plasmid #31907), IRES-tdTomato	Partially truncated commercial sequence used for initial Ca ²⁺ imaging screens; canonical protein (Q9BY67-1) in an IRES vector was used for all subsequent work
CADM1 ΔCT	N/A	N/A	PCR-based mutagenesis	IRES-tdTomato	Mutated from canonical (Q9BY67-1)
CADM1 ΔIg	N/A	N/A	PCR-based mutagenesis	IRES-tdTomato	Mutated from canonical (Q9BY67-1)
CADM1 ΔIg/ΔCT	N/A	N/A	PCR-based mutagenesis	IRES-tdTomato	Mutated from canonical (Q9BY67-1)
CADM1 ΔPDZ	N/A	N/A	PCR-based mutagenesis	IRES-tdTomato	Mutated from canonical (Q9BY67-1)
CADM4	Q8NFZ8	Horizon Discovery, ORFeome Collab.	OHS5893-202501989	IRES-mCherry	
CD55	P08174-1	Horizon Discovery, hORFeome v8.1	OHS6084-202629631	C-term 2HA, C-term mCherry (Addgene	<i>no expression</i>

				#118374, #31907)	
CD99L2	Q8TCZ2-1	Horizon Discovery, hORFeome v8.1	OHS6084- 202633259	C-term mCherry (Addgene Plasmid #31907)	Overexpression made cells unhealthy
CDH2	P19022-1	Horizon Discovery, MGC	MHS6278- 202808064	IRES-mCherry	mutations in commercial gene were corrected to the canonical sequence
CXADR	P78310-1	Horizon Discovery, hORFeome v8.1	OHS6084- 202634893	IRES-tdTomato, C-term mCherry (Addgene Plasmid #31907)	
Dsg2	O55111	Horizon Discovery, MGC	MMM1013- 211694124	IRES-tdTomato	
F11R	Q9Y624-1	Horizon Discovery, hORFeome v8.1	OHS6084- 202632205	IRES-tdTomato, C-term mCherry (Addgene Plasmid #31907)	
GPC1	P35052-1	Horizon Discovery, hORFeome v8.1	OHS6084- 202635061	IRES-tdTomato	S500G natural variant
GPC2	Q8N158	Horizon Discovery, hORFeome v8.1	OHS5893- 202494498	IRES-tdTomato	
GPC3	P51654-1	Horizon Discovery, hORFeome v8.1	OHS6084- 202635045	IRES-tdTomato	mutation in commercial gene was corrected to the canonical sequence
GPC4	O75487-1	Horizon Discovery, hORFeome v8.1	OHS6084- 202629760	IRES-tdTomato, C-term mCherry (Addgene Plasmid #31907)	
GPC5	P78333	Horizon Discovery, hORFeome v8.1	OHS6084- 202629768	IRES-tdTomato	
GPC6	Q9Y625	Horizon Discovery, hORFeome v8.1	OHS1770- 202317090	IRES-tdTomato	
IGSF8	Q969P0-1	Horizon Discovery, hORFeome v8.1	OHS6084- 202637332	IRES-tdTomato, C-term mCherry (Addgene Plasmid #31907)	
ITGA6	P23229-2	Horizon Discovery, MGC	MHS6278- 213243527	IRES-mCherry	
ITGB1	P05556-1	Horizon Discovery, MGC	MHS6278- 202757317	IRES-mCherry	<i>weak expression</i>
JAM3	Q9BX67-1	Horizon Discovery, hORFeome v8.1	OHS6084- 202633263	IRES-tdTomato, C-term mCherry (Addgene Plasmid #31907)	
KIRREL	Q96J84-1	Horizon Discovery, hORFeome v8.1	OHS6084- 202632589	C-term mCherry (Addgene Plasmid #31907)	
LMAN2	Q12907	Horizon Discovery, hORFeome v8.1	OHS6084- 202631660	IRES-tdTomato, C-term mCherry (Addgene Plasmid #31907)	

LSR	Q86X29-1	Horizon Discovery, hORFeome v8.1	OHS6084-202632381	C-term 2HA, C-term mCherry (Addgene #118374, #31907)	<i>weak expression</i>
MCAM	P43121-1	Horizon Discovery, hORFeome v8.1	OHS6084-202635261	C-term mCherry (Addgene Plasmid #31907)	
MDF1	Q99750	GenScript	gene synthesis	IRES-tdTomato	mammalian codon-optimized
NCAM1	P13591-2	Horizon Discovery, MGC	MHS6278-202802080	IRES-mCherry	Overexpression made cells unhealthy
NCSTN	Q92542-2	Horizon Discovery, hORFeome v8.1	OHS6084-202639411	C-term 2HA (Addgene Plasmid #118374)	<i>no expression</i>
NECTIN2	Q92692-2	Horizon Discovery, hORFeome v8.1	OHS6084-202630507	IRES-tdTomato, C-term mCherry (Addgene Plasmid #31907)	Transmembrane domain differs from canonical
NPTN	Q9Y639-1	Horizon Discovery, hORFeome v8.1	OHS6084-202632039	C-term mCherry (Addgene Plasmid #31907)	<i>weak expression</i>
OCLN	Q16625-1	Horizon Discovery, MGC	MHS6278-202800831	IRES-tdTomato	
PODXL	O00592-2	Horizon Discovery, hORFeome v8.1	OHS6084-202635394	C-term mCherry (Addgene Plasmid #31907)	<i>weak expression</i>
PTK7	Q13308-1	Horizon Discovery, MGC	MHS6278-202806264	IRES-mCherry	
PTPRF	P10586-2	Horizon Discovery, MGC	MHS6278-202758744	IRES-tdTomato	
PVR	P15151-1	Horizon Discovery, hORFeome v8.1	OHS6084-202635450	C-term mCherry (Addgene Plasmid #31907)	
RTN4R	Q9BZR6	Horizon Discovery, hORFeome v8.1	OHS6084-202632993	C-term 2HA (Addgene Plasmid #118374)	<i>no expression</i>
SMPDL3B	Q92485-2	Horizon Discovery, hORFeome v8.1	OHS6084-202632075	C-term mCherry (Addgene Plasmid #31907)	
TMEM30A	Q9NV96-2	Horizon Discovery, hORFeome v8.1	OHS6084-202632668	IRES-tdTomato, C-term mCherry (Addgene Plasmid #31907)	C-term construct showed an effect by Ca ²⁺ imaging, but this was not reproduced by electrophysiology. The untagged IRES vector did not have an apparent effect on PIEZO1 by Ca ²⁺ imaging or electrophysiology (Appendix II, III)

Appendix II, continued: Protein sequences for all constructs

ADAM10 (human canonical*, Uniprot ID O14672-1, 748 AA, 84.1 kDa):

MVLLRVLILLLSWAAGMGGQYGNPLNKYIRHYEGLSYNVDSLHQKHQRRAVSHEDQFSRLDFHAHGRHF
NLRMKRTDSLFSDEFKVETSNKVLGYDTSHIYTGHYGEEGSGHGSVIDGRFEGFIQTRGGTFYVEPAER
YIKDRTLPHSVIYHEDDINYPHKYGPQGGCADHSVFERMRKYQMTGVEEVVTQIPQEEHAANGPELLRKRR
TTSAEKNTCQLYIQTDLFFKYYGTREAVIAQISHVKAIIDIYQTTDFSGIRNISFMVKRIRINTTADEK
DPTNPFRFPNIGVEKFLELNSEQNHHDDYCLAHVFTDRDFDDGVGLAWVGAPSGSSGGICEKSMLYSDGKK
KSLNTGIITVQNYGSHVPPKVSHITFAHEVGHNFSPHDGSTECTPGESKNLQKENGNYIMYARATSGDK
LNNNKFSLCSIRNISQVLEKKRNNCFVESGQPICNGMVEQGEECDCGYSDQCKDECCFDANQPEGRKCKL
KPGKQCSPSQGPCATAQCAFSKSEKCRDDSDCAREGICNGFTALCPASDPKPNTDCNRHTQVCINGQCA
GSICEKYGLEECTCASSDGKDDKELCHVCCMKKMDPSTCASTGSVQWSRFSGRTITLQPGSPCNDFRGYC
DVFMRCRLVDADGPLARLKAIFSPELYENIAEWIWAHVWAVLLMGIALIMLMAGFIKICGVHTPSSNPKL
PPPPLPGTLKRRRPPQPIQQPQRQRPRESYQMGMRR

*mutations compared to canonical: L60S, D96G, S115G, Y316H, S700G; functionally characterized in Gschwind, et al. *EMBO J.* 2003, 22(10):2411(14)

ALCAM (human canonical, Uniprot ID Q13740-1, 583 AA, MW 65.1 kDa):

MESKGASSCRLLFCLLISATVFRPGLGWYTVDNSAYGDTIIIPCRLDVPQNLMGKWKYEKPDGSPVFIAFR
SSTKKSVQYDDVPEYKDRNLNSENTLSISNARISSDEKRFVCMVLVEDNVFEAPTIVKVFQPSKPEIVSK
ALFLETEQLKKLGDCISEDSYPDGNIWYRNGKVLHPLEGAVVIIFKKEMDPVTQLYTMTSTLEYKTTKAD
IQMPFTCSVTYYGPSGQKTIHSEQAQFDIYYPTEQVTIQVLPKNAIKEGDNITLKCLGNGNPPPEEFLFY
LPGQPEGIRSSNTYTLTDVRNATGDKCSLIDKSMIASTAITVHYLDLSLNPSEVTRQIGDALPVST
ISASRNATVVWMKDNIRLSSPSFSSLHYQDAGNYVCETALQEVEGLKKRESLTLLIVEGKPQIKMTKKTDP
SGLSKTIIICHVEGFPKPAIQWTITGGSVINQTEESPYINGRYSKIIISPEENVTLCTAENQLERTVNS
LNVSAISIPEHDEADEISDENREKVNDQAKLIVGIVVGLLLAAALVAGVWYLYMKSKTASKHVNKDLGNM
EENKKLEENNHKTEA

ANO6 (human canonical*, Uniprot ID Q4KMQ2-1, 910 AA, MW 106.2 kDa):

MKKMSRNVLQMEEEEDDDDGDIVLENLGQTIVPDLSLESQHDFRTPEFEEFNGKPDSLFFNDGQRRI
VLVYEDESRKETNKKGTNEKQRRKRQAYESNLICHGLQLEATRSVLDKLVFKVHAPWEVLCTYAEIMHI
KLPLKPNDLKNRSSAFGTLNWFTKVLVSDESIIKPEQEFFTAPFEKNRMNDYIVDRDAFFNPATRSRIVY
FILSRVKYQVINNSKFGINRNLVNSGIYKAAFLHDCKFRQSEDPCPNERYLLYREWAHPRSIYKKQPL
DLIRKYYGEKIGIYFAWLGYYTQMLLAAVVGACFLYGYLNQDNCTSKEVCHPDIGGKIIMCPQCDRLC
PFWKLNITCESSKLCIFDSFGTLVFAVFMGVWVTLFLEFWKRRQAELEYEWDTVELQQEEQARPEYEARC
THVVINEITQEEERIPFTAWGKCIRITLCASAVFWILLIIASVIGIIVYRLSVFIVFSAKLPKNINGTDP
IQKYLTPQTATSITASIISFIIIMILNTIYEKVAIMITNFELPRTQTDYENSITMKMFLQFVNYYSSCFY
IAFFKGKFGVGYPGDPVYWLGYRNECDPGGCCLLELTQTLTIMGKAIWNNIQEVLLPWIMNLLIGRFHRV
SGSEKITPRWEQDYHLQPMGKGLFYEYLEMIIQFGFVTLFVASFPLAPLLALVNNILEIRVDAWKLTQF
RRLVPEKAQDIGHAQWQPMQGIAILAVVTNAMIIAFTSDMIPRLVYYWSFVPPYGDHTSYTMEGYINNTLS
IFKVADFKNKSKGNPYSDLGNHTTCRYDFRYPPGHQEYKHNIYYWHVIAAKLALIIVMEHVIYSVKFFI
SYAIPDVSKRTKSKIQREKYLTKLHENHLKDMTKNMGVIAERMIEAVDNNLRPKSE

*contains F837L point mutation relative to canonical

ANO6 (mouse canonical, Uniprot ID Q6P9J9-1, 911 AA, MW 106.3 kDa):

MQMMTRKVLLNMELEEDDDEDGDIVLENFDQTVCPFGSLENQQDFRTPEFEEFNGKPDSLFFTDGQRRI
DFILVYEDESKKENKKGTNEKQKRKRQAYESNLICHGLQLEATRSVSDDKLVFKVHAPWEVLCTYAEIM

HIKLPLKPNDLKTRSPFGNLNWFTKVLRVNESVIKPEQEFTAPFEKSRMNDYILDRTDSFFNPATRSRIV
YFILSRVKYQVMNNVNKGINRLVSSGIYKAAPPLHDCRFNYESEDISCPSERYLREWAHPRSIYKKQP
LDLIRKYYGEKIGIYFAWLGGYTQMLLAAVVGACFLYGYLDQDNCTWSKEVCDPDIGGQILMCPCDRL
CPFWRNLNTCESSKKLCIFDSFGTLIFAVFMGVWTLFLEFWKRRQAELEYEWDTVELQQEEQARPEYEAQ
CNHVVINEITQEERIPTTCGKCIRVTLCASAVFFWILLIASVIGIVYRLSVFIVFSTTLPKNPNGTD
PIQKYLTQPQMATTSITASIISFIIMILNTIYEKVAIMITNFELPRTQTDYENSLSMKMFLFQFVNYYSSCF
YIAFFKGKFVGYPDPVYLLGKYRSEECDPGGCLLETTQLTIIMGGKAIWNNIQEVLPPVMNLIGRYKR
VSGSEKITPRWEQDYHLQPMGKGLFYEYLEMIIQFGFVTLFVASFPLAPLLALVNNILEIRVDWKLTQ
FRRMVPEKAQDIGAWQPIMQGIAILAVVTNAMIJAFTSDMPIRLVYYWSFSIPPYGDHTYYTMGYINNTL
SVFNITDFKNTDKENPYIGLGNYTLCRYRDFRNPPGHQEKHNIIYWHVIAAKLAFIIVMEHIIYSVKFF
ISYAIPDVSKITSKIKREKYLTKLLHESHLKDLSKMGIIAERIGGTVDNSVRPKLE

ATP1B1 (human canonical, Uniprot ID P05026-1, 303 AA, 35.1 kDa):

MARGKAKEEGSWKKFIWNSEKKEFLGRTGGSWFKILLFYVIFYGCLAGIFIGTIQVMLLTISEFKPTYQDR
VAPPGLTQIPQIQKTEISFRPNPDKSYEAYVNLNIVRFLEKYKDSAQRDMDIFEDCGDVPSEPKERGDFNHE
RGERKVCRFKLEWLGNCGLNDETYGYKEGKPCIIKLNRLVLFKPCKPKNESLETYPVMKYNPNVLPVQC
TGKRDEDKDKVGNVEYFGLGNSPGFPLQYYPYGKLLQPKYLQPLLAQFTNLTMDTEIRIECKAYGENIG
YSEKDRFQGRFDVKIEVKS

BCAM (human canonical, Uniprot ID P50895, 628 AA, 67.4 kDa):

MEPPDAPAQARGAPRLLLAVLLAAHPDAQAEVRLSVPLVEVMRGKSVILDCTPTGTHDHYMLEWFLTDR
SGARPRLASAEMQGSELQVTMHDTRGRSPYQLDSQGRVLVLEAQVGDERDYCVVRAGAAGTAATARLN
VFAKPEATEVSPNKGTLCSVMEDSAQEIACTCSRNGNPAPKITYWYRNGQRLEVPEVMNPEGYMTSRTVREAS
GLLSLTSTLYLRLRKDDRDASFCAAHYSLPEGRHGRLDSPTFHLLHYPTEHVQFWVGPSTPAGWVREG
DTVQLLCRGDGSPSPEYTLFRLQDQEVEVLNVNILEGNLTLEGVTRGQSGTYGCRVEDYDAADDVQLSKTLE
LRVAYLDPLELSEGKVLSLPLNSSAVVNCVHGLPTPALRWTKDSTPLGDGPMLSLSITFDNGTYVCEA
SLPTPVPLSRTQNTLLVQGSPELKTAIEPKADGSWREGDEVTLICSGRHPDPKLSWSQLGGSPAEPPIP
GRQGWVSSSLTLKVTALS RDGISC EA SNPHGNKRHV FGT VSP QAGV A VMA VAV SVG LLL LVV AVF
YCVRRKGGPCCRQREKGAPPGEPLSHGSEQEQTGLLMGGASGGARGGSGGFDEC

CADM1 (human canonical, Uniprot ID Q9BY67-1, 442 AA, MW 48.5 kDa):

MASVVLPSGSQCAAAAAAAPPGRLRLLLLLFSAAALIPTGDGQNLFTKDVTVIEGEVATISCVNKSD
SVIQLLNPNRQTIYFRDFRPLKDSRFQLLNFSSSELKVSLTNVSISDEGRYFCQLYTDPPQESYTTITVLV
PPRNLMDIQKDTAVEGEIEVNCTAMASKPATTIRWFKGNTTELKGKSEVEEWSDMYTVTSQMLKVHKED
DGVPVICQVEHPAVTGNLQTQRYLEVQYKPQVHIQMTPYPLQGLTREGDALELTCEAIGKPQPVMTWVRVD
DEMPQHAVLSPNLFINNLNKT DNG TYRCEASNIVGKAHS DYML YVYD PPT TIP PTTTTTTTTT
TIITDSRAGEEGSIRAVDHAVIGGVAVVFAMLCLLIILGRYFARHKGTYFTHEAKGADDAADATAIIN
AEGGQNNEEKKEYFI

CADM1 (human truncated isoform*, Uniprot ID A0A4Z1, 387 AA, MW 42.7 kDa):

MASVVLPSGSQCAAAAAAAPPGRLRLLLLLFSAAALIPTGDGQNLFTKDVTVIEGEVATISCVNKSD
SVIQLLNPNRQTIYFRDFRPLKDSRFQLLNFSSSELKVSLTNVSISDEGRYFCQLYTDPPQESYTTITVLV
PPRNLMDIQKDTAVEGEIEVNCTAMASKPATTIRWFKGNTTELKGKSEVEEWSDMYTVTSQMLKVHKED
DGVPVICQVEHPAVTGNLQTQRYLEVQYKPQVHIQMTPYPLQGLTREGDALELTCEAIGKPQPVMTWVRVD
DEMPQHAVLSPNLFINNLNKT DNG TYRCEASNIVGKAHS DYML YVYD S RAGE EG SIR AV DH AV IGG V V AV
VVFAMLCLLIILGRYFARHKGFLSLTSPRIK

*commercially available gene from ORFeome library that contains a C-terminal truncation; this sequence was used only for preliminary calcium imaging screening prior to gene synthesis and subcloning of the canonical sequence.

CADM1 ΔCT (C-terminal deletion mutant Δ401–442):

MASVVLPSGSQCAAAAAAAPPGLRLRLLLLLFSAAALIPTGDGQNLFTKDVTVIEGEVATISCVNKSD
SVIQLLNPNRQTIYFRDFRPLKDSRFQLLNFSSSELKVSLTNVISDEGRYFCQLYTDPPQESYTTITVL
PPRNLMIDIQKDTAVEGEIEEVNCTAMASKPATTIRWFKGNTELKGKSEVEEWSDMYTVTSQMLKVHKED
DGVPVICQVEHPAVTGNLQTQRYLEVQYKPKQVHIQMTPQGLTREGDALELTCEAIGKPQPMVTWVRD
DEMPQHAVLSGPNLFINNLNKTNGTYRCEASNIVGKAHSYDMLYVYDPPTTIPPPTTTTTTTTTIL
TIIITDSRAGEEGSIRAVDHAVIGGVVAVVFAMLCLLIILGRYFA

CADM1 ΔIg (Ig domain deletion mutant Δ59–316):

MASVVLPSGSQCAAAAAAAPPGLRLRLLLLLFSAAALIPTGDGQNLFTKDVTVIEGEGETNIVGKAHSYD
LYVYDPPTTIPPPTTTTTTTILTIITDSRAGEEGSIRAVDHAVIGGVVAVVFAMLCLLIILGRY
FARHKGTYFTHEAKGADDAADADTAIINAEGQNSEEKEYFI

CADM1 ΔIg/ΔCT:

MASVVLPSGSQCAAAAAAAPPGLRLRLLLLLFSAAALIPTGDGQNLFTKDVTVIEGEGETNIVGKAHSYD
LYVYDPPTTIPPPTTTTTTTILTIITDSRAGEEGSIRAVDHAVIGGVVAVVFAMLCLLIILGRY
FA

CADM1 ΔPDZ (PDZ-binding domain deletion mutant Δ440–442):

MASVVLPSGSQCAAAAAAAPPGLRLRLLLLLFSAAALIPTGDGQNLFTKDVTVIEGEVATISCVNKSD
SVIQLLNPNRQTIYFRDFRPLKDSRFQLLNFSSSELKVSLTNVISDEGRYFCQLYTDPPQESYTTITVL
PPRNLMIDIQKDTAVEGEIEEVNCTAMASKPATTIRWFKGNTELKGKSEVEEWSDMYTVTSQMLKVHKED
DGVPVICQVEHPAVTGNLQTQRYLEVQYKPKQVHIQMTPQGLTREGDALELTCEAIGKPQPMVTWVRD
DEMPQHAVLSGPNLFINNLNKTNGTYRCEASNIVGKAHSYDMLYVYDPPTTIPPPTTTTTTTIL
TIIITDSRAGEEGSIRAVDHAVIGGVVAVVFAMLCLLIILGRYFARHKGTYFTHEAKGADDAADADTAIIN
AEGQNSEEKKE

CADM4 (human canonical, Uniprot ID Q8NFZ8, 388 AA, 42.8 kDa):

MGRARRFQWPLLLWAAAAGPGAGQEVQTEVENTVAEGGVAEITCRLHQYDGSIVVIQNPARQLFFNGTRA
LKDERFQLEEFSPRRVRIRLSDARLEDEGGYFCQLYTEDTHQIATLTVLAPENPVVEVREQAVEGGEVE
LSCLVPRSRPAATLWRYDRKELKGVSQQENGKVWSVASTVRFRVDRKDGGIIICEAQNQALPSGHSKQ
TQYVLVDQYSPTARIHASQAVVREGDTLVLTCAVTGNPRPNQIRWNRGNESLPERAEAVGETLTLPGLVSA
DNGTYTCEASNKHGHARALYLVVYDPGAVVEAQTSVPYAIVGGLALLVFLICVLVGMVCSVQKGSY
LTHEASGLDEQGEAREAFLNGSDGHKRKEFFI

CD55 (human canonical, Uniprot ID P08174-1, 381 AA, MW 41.4 kDa):

MTVARPSVPAALPLLGELPRLLLVLLCLPAVGDCGLPPDVPNAQPALEGRTSFPEDTVITYKCEESFKV
IPGEKDSVICLKGSQWSDIEEFCNRSC EVPTRLN S ASLKQPYITQNYFPVGTVEYE CRPGYRREPSLSPK
LTCLQNLKWSTAVEFCKKKSCP NGEIRNGQIDVPGGILFGATISFS CNTGYKLFGSTSSFC LISGSSVQW
SDPLPECREIYCPAPPQIDNGIIQGERDHYGYRQS VTYACNK GFTMIGEH SIYCTVN DEGEWSGPPPECR
GKS LTKVPP TVQKPTVNVPTTEVSP TSQ KTTT PNAQATRSTP VSRTKHF HETTPNKGSGTTSGT
TRLLSGHTCFTLTGLLGTLVTMGLT

CD99L2 (human canonical, Uniprot ID Q8TCZ2-1, 262 AA, 28.0 kDa):

MVAWRSAFLVCLAFSLATLVQRGSGDFDDFNLEDAVKETSSVKQPWDHTTTTNRPGTTRAPAKPPGSGL
DLADALDDQDDGRKPGIGGRERWNHVTTTKRPVTRAPANTLGNDFDLADALDDRNDRDRDGRRKPIAGG
GGFSDKDLEDIVGGEYKPDKGKDGRYGSNDDPGSGMVAEPTIAGVASALAMALIGAVSSYISYQQKKF
CFSIQQGLNADYVKGENLEAVVCEEPQVKYSTLHTQSAEPPPPEPARI

CDH2 (human canonical, Uniprot ID P19022-1, 906 AA, MW 99.8 kDa):

MCRIAGALRTLLPLLAALLQASVEASGEIALCKTGFPEDVYSAVLSDVHEGQPLNVKFSNCNGKRKVQY
ESSEPADFKVDEDGMVYAVRSFPLSSEHAKFLIYAQDKETQEKWQAVKLSLKPTLTEESVKESAEVEEIV
FPRQFSKHSGLQRQKRDWVIPPINLPENSRGPFQELVRIRSDRKNLRLRYSVTGPQADQPPTGIFIIN
PISGQLSVTKPLDREQIARFHRLRAHAVDINGNQVENPIDIVINVIDMNDNRPEFLHQVWNGTVPEGSKPGT
YVMVTATAIDADDPNALNGMLRYRIVSQAPSTPSPNMFTINNETGDIITVAAGLDREKVQQYTLIIQATDME
GNPTYGLSNTATAVITVTDVNDNPEFTAMTFYGEVPENRVDIIVANLTVDKDQPHPAWNAVYRISGGD
PTGRFAIQTDPSNDGLTVVKPIDFETNRMFVLTVAARENQVPLAKGIQHPPQSTATSVTVIDVNENPYF
APNPKIRQEEGLHAGTMLTFTAQDPDRYMQQNIRYTKLSDPANWLKIDPVNGQITTIAVLDRESPNVKN
NIYNATFLASDNGIPPMSTGTQIYLLDINDNAPQVLPQEAETCETPPDNSINITALDYDIDPNAGPFAF
DLPLSPVTIKRNWTITRLNGDFAQLNLKIKFLEAGIYEVPPIITDSGNPPKSNISILRVKVCQCDSDNGDCT
DVDRIVGAGLGTGAIIAILLCIIILLILVLMFVWMKRRDKERQAKQLLIDPEDDVRDNILKYDEEGGGE
DQDYDLSQLQQPDTEVPDAIKPGVIRRDERPIHAEPQYPVRSAAHPGDIGDFINEGLKAADNDPTAPPY
DSLLVFDYEGSGSTAGSLSSLNSSSGEQDYDYLNDWGPRFKKLADMYGGDD

CXADR (human canonical, Uniprot ID P78310-1, 365 AA, 40.0 kDa):

MALLLCFVLLCGVVFARSLSITTPPEEMIEKAKGETAYLPCKFTLSPEDQGPLDIEWLISPADNQKVDQVI
ILYSGDKIYDDYYPDLKGRVHTSNDLKGDSASINVNLQLSDIGTYQCKVKKAPGVANKKIHLVVLVVKPS
GARCYVDGSEEIGSDFKIKCEPKEGSLPLQYEWQKLSQKMPSTSWEAHTSSVISVKNASSEYSGTYSCT
VRNRVGSDQCLLRNVPVPSNKAGLIAGAIITGLLALALIGLIIFCCRKKRREEKYEKEVHHDIRDVPPP
KSRTSTARSYIGSNHSSLGMSMSPSNMEGYSKTQYNQVPSDEFERTPQSTPLPPAKVAAPNLSRMGAIPVMI
PAQSKDGSIV

DSG2 (mouse canonical, Uniprot ID O55111, 1122 AA, MW 122.4 kDa):

MARSPGDRCALLLVQLLAVVCLDFGNGLHLEVFSRNEGKPFKPHTHLVRQKRAWITAPVALREGEDLSR
KNPIAKIHSDLAEKGKIKITYKTYGKITEPPFGIFVFDRNTGELNITSILDREETPYFLLGYALDSRGN
NLEKPLELRIKVLDINDNEPVFTQEVFVGSIEELSAHTLVMKITATDADDPETLNAKVSYRIVSQEPANS
HMFYLNKDTGEIYTTSTLDREEHSSYLTVEARDNGQITDKPVQQAQVQIRILDVNDNIPVVENKMYEG
TVEENQNVEMVRIKVTDADEVGSNDNWLANTFASGNEGYYHIETDTQTNEGIVTUVKEVDYEEMKL
SIIVTNKAAPHKSILSKYKATPIPITVKVKNVVEGIHFKSSVVSFRASEAMDRSSLSRSIGNFQVFDEDTG
QAAKVTYVKVQDTDNWVSVDSVTSEIQLVKIPDFESRYVQNGTYTAKVVAISKEHPQKTITGTIVITVEDV
NDNCPVLVDSVRSCEDEPYVNTAEDLDGAQNSAPFSFSIDQPPGTAAQKWKITHQUESTVLLQQSERKR
GRSEIPFLISDSQGFSCPERQVLQLTVCECLKGGCVAAQYDNYVGLGPAIALMILALLLLL
CHCGGGAKGFTPIPGTIEMLHPWNNEGAPPEDKVVPSLLVADHAESSAVRGGVGGAMLKEGMMKGSSASV
TKGQHELSEVDGRWEEHRSLLTAGATHVRTAGTIAANEAVRTRATGSSRDMSGARGAVAVNEEFLRSYFT
EKAASYNGEEDLHMAKDCLLVSQEDTASLRGSVGCCSFIEGELDDLFDDLGKFTLAEVCLGRKIDLD
VDIEQRQKPVREASVSAASGSHYEQAVTSSESAYSSNTGFPAKPLHEVHTEKVTQEIVTESSVSSRQSQK
VVPPPDVVASGNIIVTETSYAKGSAVPPSTVLLAPRQPQSLIVTERVYAPTSTLVDQHYANEEKVLTERV
IQPNGGIPKPLEVTQHLKDAQYVMVRERESILAPSSGVQPTLAMPSVAAGGQNVTTERILTPASTLQSSY
QIPSETSETARNTVLSSVGSIGPLPNLDLEESDRPNSTITSSSTRVTKHSTMQHSYS

F11R (human canonical, Uniprot ID Q9Y624-1, 299 AA, MW 32.6 kDa):

MGTKAQVERKLLCLFILAIIICSLALGSVTVHSSEPEVRIPENNPVKLSCAYSGFSSPRVEWKFDQGDTTR
LVCYNNKITASYEDRVTFPLPTGITFKSVTREDTGYTCMVSEEGGNSYGEVKVLIVLVPPSKPTVNIPSS
ATIGNRAVLTCSQDGSPSEYTWFKDGVIMPTNPKSTRAFSNSSYVILNPTTGELEVFDPLSASDTGEYSCE
ARNGYGTPMTSNAVRMEAVERNVGIVAAVLTLILLGILVFGIFWFAWSRGHFDRTKKGTSSKKVIYSQPS
ARSEGEFKQTSFLV

GPC1 (human canonical*, Uniprot ID P35052-1, 558 AA, MW 61.7 kDa):

MELRARGWWLLCAAAALVACARGDPASKSRSCGEVRQIYGAKGFSLSDPVQAEISGEHLRICPQGYTCCTS
EMEENLANRSHAELETALRDSSRVLQAMLATQLRSFDDHFQHLLNDERTLQATFPGAFGELYTQNARAFR
DLYSELRLYYRGANLHLEETLAEFWARLLERLFKQLHPQLLLPPDDYLDCLGKQAEALRPFGEAPRELRLRA
TRAFVAARSFVQGLGVASDVVRKVAQVPLGPECSRAVMKLVYCAHCLGVPGARPCPDYCRNVLKGClanqa
DLDAEWRNLLDSMVLITDKFWGTSGVESVIGSVHTWLAEAINALQDNRTLTAKVIQCGGNPKVNPQGP
EEKRRRGKLAPEPRRPPSGTLEKLVSEAKAQLRDVQDFWISLPGTLCSEKMASTASDDRCWNGMARGRYLP
EVMGDGLANQINNPEVEVDITKPDMTIRQQIMQLKIMTNRLRSAYNGNDVFDQDASDDGSGSGSGDGLDD
LCGRKVSRKSSSSRTPLTHALPGLSEQEQKTSAASCPQPPTFLPLFLALTVARPRWR

*S500G natural variant

GPC2 (human canonical, Uniprot ID Q8N158, 579 AA, MW 62.8 kDa):

MSALRPLLLLLPLCPGPAGPGSEAKVTRSCAETRQVLGARGYSLNLIppalISGEHLRVCpqeytccss
ETEQRLIRETEATFRGLVEDSGSFLVHTLAARHRKFDEFFLEMLSVAQHSLTQLFSHSYGRlyaqhalifn
GLFSRLRDFYGESGEGLDDTLADFWAQLLERVFPLLHPQYSFPPDYLLCLSRLASSTDGSLQPFgdsprrl
RLQITRTLVAARAFVQGLETRNVVSEALKPVSEGSQALMRLIGCPLCRGVPSLMPCQGFCLNVVRGCL
SSRGLEPDWGNYLdglliladklqgpfsfeltaesigvkiseglmylqensakvsaqvfqecgppdpvppar
NRRAPPREEAgrlwmvtEEERPTTAAGTNHRLVWELRERLARMGFwarlsLTVCgdsrmaadaslea
APCWTGAGRGRYLPVVGGSPAqvnnpelkvdaSGPDVPTRRRLQlaatarmktaalghdldgqda
DASGSGGGQQYADDWMAGAVAPPARPPRPPYPPrrdgsGGKGgggsarynqrsrsGGASIGFHTQTILIL
SLSALALLGPR

GPC3 (human canonical, Uniprot ID P51654-1, 580 AA, MW 65.6 kDa):

MAGTVRTACLVVAMLLSLDFPGQAQPpppppdTATCHQVRSFFORLQPGlkwvpPETPVPGSDLQVCLPKGPT
CCSRKMEEKYQLTARLNMEQLQSASMElkfliiqnaafvqeaFEIVVRHAKNYTNAMFKNNYPSLTPQAF
EFVGEFTDVSLYIlgSDINVDDMVNEfdslfpviytqlmnpglpsaldineclrgarrdlkvfgnfpk
LIMTQVSKSLQVTRIFLQALNLGIEVINTTDHLKFSKDCGRMLTRMWYCSYCQGLMMVKPCGGYCNVVMQG
CMAGVVEIDKYWREYIlslelvngmyriydmenvllglfstihdsiqqvqknagklTTTIGKLCahsqr
QYRSAYYPedlfidkkvlkvahveheetlssrrrelIQKLKSfisfysalpgyicshspvaendtlcwngq
ELEVERYSQKAARNGMKNQFNnlhelkmkgpepvvsqiidklkhinqlrtmsmpkgrvldknlddeefgesgd
CGDDEDECigsgdgmikvknqlrflaelayldvdapgnsqqatpkdneistfhnlgnvhsplklltsm
AISVVCFFFLVH

GPC4 (human canonical, Uniprot ID O75487-1, 556 AA, MW 62.4 kDa):

MARFGLPALLCTLAVLSAALLAAELKSKCSEVRRLYVSKGFNKNDAPLHEINGDHLKICPQGSTCCSQEM
EEKYSLQSKDDFKSVVSEQCcnhlqavfasrykkfDEFFKELENAEKSlndmfVKTYGHLYMQNSELFfkdl
FVELKRYYVVGvnvnleemlnDFWARLLERMFrlvnsqyhftDEYLECVSKYteqlkpfgdvprklklqvtr
AFVAARTFAQGLAVAGDVvskvsvnptaqcthallkmiycshcrglvtkpccyncsnimrgclanqgdl
DFEWNNFidamlmvaeerleggpfniesvmdpidvkksdaimnmqdnsvqsvsqvfqgcgppkplpagrisrs
ISESAFSARFRPHPEERPTTAAGTtsldrlntdvkeklqakkfwsslpsncndermaagngneddcwng

KGKSRYLFAVTGNGLANQGNNEVQVDTSKPDILILRQIMALRVMTSKMKNAYNGNDVFFDISDESSGEG
SGSGCEYQQCPSEFDYNATDHAGKSANEKADSAGVRPGAQAYLLTVFCILFLVMQREWR

GPC5 (human canonical, Uniprot ID P78333, 572 AA, MW 63.7 kDa):

MDAQTWPVGFRCLLLLALVGSARSEGVTCEEVRLFQWRLLGAVRGLPDSPRAGPDLQVCISKKPTCCTR
KMEERYQIAARQDMQQLQTSSTLKFISRNAAAFQETLETLIKQAENYTSILFCSTYRNMALEAAASVQ
EFFTDVGLYLFGADVNPEEFVNRRFDLSFLPVNHЛИНPGVTDSSLEYSECIRMARRDVSPFGNIPQRVMG
QMGRSLLPSRTFLQALNLGIEVINTTDYLHSKECSRALLKMQYCPHCQGLALTCKPCMGYCLNVMRGCLAH
MAELNPHWHAYIRSLEELSDAMHGTYDIGHVLLNFHLLVNDAVLQAHNGQKLLEQVNRICGRPVRTPTQS
PRCSFDQSKEKHGMKTTTRNSEETLANRRKEFINSRLYRSFYGLADQLCANELAAADGLPCWNGEDIVK
SYTQRVGNGNIKAQSGNPEVKVKGIDPVINQIIDKLKHVVQLLQGRSPKPKWELLQLGSGGGMVEQVSGD
CDDEDCGGGSGSGEVKRTLKITDWMPDDMNFS DVKQIHQTDGSTLTTGAGCAVATESMTFTLISVVMLL
PGIW

GPC6 (human canonical, Uniprot ID Q9Y625, 555 AA, MW 62.7 kDa):

MPSWIGAVILPLLGLLSLPAGADVAKARSCGEVRQAYGAKGFSLADIPIYQEIAGEHLRICPQEYTCCTTEM
EDKLSQSKLEFENLVEETSHFVRTTFSRHKKFDEFFRELLENAEKSNDMFVRTYGMLYMQNSEVFQDL
FTELKRYYTGGNVNLEEMLNDFWARLLERMFQLINPQYHFSEDYLECVSKYTDQLKPGDVPRKLKIQVTR
AFIAARTFVQGLTVGREVANRVSKSPTPGCIRALMKMLYCPYCRGLPTVRPCNNYCLNMKGCLANQADL
DTEWNLFIDAMLLVAERLEGPFNIESVMDPIDVKISEAIMNMQENSMQVSAKVFQGCGQPKPAPALRSARS
APENFNTRFRPYNPEERPTTAAGTSLDRLVTDIKEKLKLSKKVWSALPYTICKDESVTAGTSNEECWNHG
SKARYLPEIMNDGLTNQINNPEVDVDIRPDTFIRQQIMALRVMTNKLKNAYNGNDVNFQDTSDESSGSGS
GSGCMDDVCPTEFVTTEAPAVDPDRREVDSAAQRGHSSLWSLTCIVLALQRLCR

IGSF8 (human canonical, Uniprot ID Q969P0-1, 613 AA, MW 65.0 kDa):

MGALRPTLLPPSLPLLLLLMLGMGCWAREVLVPEGPLYRVAGTAVSISCNVTGYEGPAQQNFEWFLYRPEA
PDTALGIVSTKDTQFSYAVFKSRVVAGEVQVQRLQGDAVVLKIARLQAOQDAGIYECHTPSTDTRYLGSYSG
KVELRVLPDVQVSAAPPGPRGRQAPTSPPRMTVHEGQELALGCLARTSTQKHThLAWSGRSVPEAPVGR
STLQEUVGIRSDLAVEAGAPYAERLAAGELRLGKEGTDYRMVVGGAQAGDAGTYHCTAAEWIQDPDGSWA
QIAEKRAVLAHVDTVQTLSSQLAVTVPGERRIGPGEPLELLCNVSGALPPAGRHAAYSVGWEMA PAGAPGP
GRLVAQLDTEGVGSLGPGYEGRHIAMEKVASRTYRLREAARPGDAGTYRCLAKAYVRSGTRLREAASAR
SRPLPVHVREEGVVLEAVAWLAGGTYRGETASLLCNISVRGGPPGLRLAASWWVERPEDGELESSVPAQLV
GGVGQDGVAELGVVRPGGGPVSELVGPRSHRLRLHSLGPEDEGVYHCAPS A伟VQHADYSWYQAGSARSGPV
TVYPYMHALDTLFVPLLVTGVALVTGATVLGTITCCFMKRLRKR

ITGA6 (human isoform Alpha-6X1A*, Uniprot ID P23229-2, 1073 AA, 119.5 kDa):

MAAAGQLCLLYLSAGLLSRLGAAFNLDTREDNVIRKYGDPGSLFGFSLAMHWQLQPEDKRLLLVGAPRAEA
LPLQRANRTGGLYCDITARGPCTRIEFDNDADPTSESKEDQWMGTVQSQGPGGVVTCAHRYEKRQHVN
TKQESRDIFGRCYVLSQNLRIEDDMGGSFCGRLRGHEKFGSCQQGVAATFTKDFHYIVFGAPGTYNW
KGIVRVEQKNNTFDMNIFEDGPYEVGGETEHDES LVPVPANSY LGFSLDSGKGIVSKDEITFVSGAPRAN
HSGAVVLLKRDMSKAHLLPEHIFDGEGLASSFGYDVAVVDLNKDGWQDIVIGAPQYFDRGEVGGAVYVYM
NQQGRWNNVKPIRLNGTKDSMFGITVKNIGDINQDGYPDIAVGAPYDDLGVFIYHGSANGINTKPTQVLK
GISPYFGYIAGNMDLDRNSYPDVAVGSSLSDSVTIFRSRPVINIQKTITVTPNRIDLQKTAGAPSGICL
QVKSCFEYTANPAGYNPSISIVGTLEAEKERRKSGLSSRVQFRNQGSEPKYTQELTLRKQKQKVCMEETLW
LQDNIRDKLRPIPITASVEI QEPSSRRVNSLPEVLPILNSDEPKTAHIDVHFLKECGDDNCNSNLKLE
YKFCTREGNQDKFSYLPPIQKGVPELVLDQKDIALEITVTPSNPRNPTKDGDDAHEAKLIATFPDTLY
SAYRELAPEKQLSCVANQNGSQADCELGNPFKRNSNVTFLVLSSTTEVTFDTPLDINLKLETTSNQDN
LAPITAKVVIELLSVSGVAKPSQVYFGGTVVGEQAMKSEDEVGSLIEYEFRVINLGKPLTNLTATLN
IQWPKEISNGKWLLYLVKVESKGLEKVTCEPQKEINSLNLTESHNSRKKREITEKQIDDNRKFSLFAERKY
QTLNCCSVNVNCVNRCPRLGLDSKASLILRSRLWNSTFLEEYSKLNYLDILMRAFIDVTAAENIRLPNAG

TQVRVTVFPSKTVAQYSGVPWWIILVAILAGILMLALLVFIWKCGFFKRNKKDHYDATYHKAEIHAQPSD
KERLTSDA

*Most similar to Alpha-6X1A, differences compared to canonical: Δ255–293, A419T, 1084–1130
SRYDDSVPRYHAVRIRKEEREIKDEKYIDNLEKKQWITKWNENESYS → NKKDHYDATYHKAEIHAQPSD
AQPSDKERLTSDA

ITGB1 (human canonical, Uniprot ID P05556-1, 798 AA, 88.4 kDa):

MNLQPIFWIGLISSVCCVFAQTDENRCLKANAKSCGECIQAGPNCWGCTNSTFLQEGMPTSARCDDLEALK
KKGCPPDDIENPRGSKDIKKKNVTNRSGTAEKLKPEDITQIOPQQVLRLRSGEPQTFTLKFRAEDYP
IDLYYLMDSLSSMKDDLENVKSLGTDLNMEMRRITSDFRIGFGSFVEKTVMPYISTTPAKLRNPCTSEQNC
TSPFSYKNVLSLTNKGEVFNELVGKQRISGNLDSPEGGFADIMQAVCGSLIGWRNVTRLLVFSTDAGHF
AGDGKLGIVLPNDGQCHLENNMYTMSSHYYDYPSSIAHLVQKLSENNIQTIFAVTEEFQPVYKELKNLIPKS
AVGTLSANSSNVNIQLIIDAYNSLSSEVILENGLSEGVTISYKSYCKNGVNGTGENGRKCSNISIGDEVQF
EISITSNKCPKDKSDSFKIRPLGFTEEVEILQYICECECQSEGIPESPKCHEGNGTFECGACRCNEGRVG
RHCECSTDEVNSEMDAYCRKENSSEICSNNGECVCGQCVCRKRDNTNEIYSGKFCECDNFNCDRSNGLIC
GGNGVCKCRVCECNPNYTGSACDCSLDTSTCEASNGQICNGRGICECGVCKCTDPKFQGQTCEMCQTCCLGV
CAEHKECVQCRAFNKGEEKDCTQECSYFNITKVESRDKLPQPQPDVSHCKEVDCCWFYFTYSVNGN
NEVMVHVVENPECPTGPDIPIVAGVVAGIVLIGLALLIWKLLMIIDRREFAKEKEKMNAKWDTGENP
IYKSAVTVVNPKYEGK

JAM3 (human canonical, Uniprot ID Q9BX67-1, 310 AA, MW 35.0 kDa):

MALRRPRLCARLPDFFLLLFRGCLIGAVNLKSSNRTPVVQEFESELSCIITDSQTSDPRIEWKKIQ
DEQTTVYFFDNKIQGDLAGRAEILGKTSLSKIWNVTRRDSALYRCEVVARNDRKEIDEIVIELTVQVKPVTP
VCRVPKAVPGKMATLHCQESEGHPRPHYSWYRNDVPLPTDSRANPRFRNSSFHLNSETGLVFTAHKDD
SGQYYCIA SNDAGSARCEEQEMEVYDLNIGGIIGGVLVLAVALITALTGICCAYRRGYFINNKQDGESYKN
PGKPDGVNYIRTDEEGDFRHKSSFVI

KIRREL (human canonical, Uniprot ID Q96J84-1, 757 AA, 83.5 kDa):

MLSLLWILTLSDTFSQGTQTRFSQEPADQTVAGQRAVLPVCVLLNYSGIVQWTKDGLALGMQGLKAWPR
YRVVGSADAGQYNLEITDAELSDDASYECQATEAALRSRAKLTVLIPPEDTRIDGGPVILLQAGTPHNL
CRAFKPAATIIWFRDGTQEGAVASTELLKGKRETTVSQLLINPTLDIGRVTCSRSMNEAIPSGKET
SIELDVHHPPVTLSIEPQTVQEGERVVFTCQATANPEIILGYRWAKGFLIEDAHESRYETNDYSFFTEP
VSCEVHNKVGSTNVSTLVNVHFAPRIVDPKPTTDIGSDVTLTCVWVGNPLTLTWTKKDSNMVLSNSNQ
LLLKSVTQADAGTYTCRAIIVPRIGVAEREVPLYVNGPPIISSEAVQYAVRGDGKVEFIGSTPPPDRIAW
AWKENFLEVGTLEYRTVERTNSGSGVLSTLTINNMEADFQTHYNCTAWSNSFGPGTATIQLEREVLPVGI
IAGATIGASILLIFFFIALVFFLYRRRKGSRKDVTLRKLDIKVETVNREPLTMHSREDDTASVSTATRM
KAIYSSFKDDVDLKQDLRCDTIDTREEEYEMKDPTNGYYNVRAHEDRPSSRAVLYADYRAPGPARFDGRPSS
RLSHSSGYAQINTYSRGPASDYGPEPTPPGPAAPAGTDTSQLSYENYEKFNSHPFGAAGYPTYRLGYPQ
APPGLERTPYEAYDPIGKYATATRFSYTSQHSYQRFQQRMQTHV

LMAN2 (human canonical, Uniprot ID Q12907, 356 AA, MW 40.2 kDa):

MAAEGWIWRWGWRRCCLGRPGLLGPBPPTPLFLLLLLGSVTADITDGNSEHLKREHSLIKPYQGVGSS
MPLWDFQGSTMLTSQYVRLTPDERSKEGSIWNHQPCFLKDWEHVHFVHGKGKKNLHGDIALWYTRDRL
VPGPVFGSKDNFHGLAIFLDTYPNDETERVFPYISVMVNNGSLSYDHSKDGRWTELAGCTADFRNRDHT
FLAVRYSRGRLTVMTDLEDKNEWKNCIDITGVRLPTGYYFGASAGTGDLSDNHDISMKLFQLMVEHTPDE
ESIDWTKIEPSVNFLKSPKDNVDDPTGNFRSGPLTGWRVFLLLCA LLGIVVCAVVGAVVFQKRQERNKRF
Y

LSR (human canonical, Uniprot ID Q86X29-1, 649 AA, MW 71.4 kDa):

MQQDGLGVGTRNGSGKGRSVHPSWPWCAPRPLRYFGRDARARRAQTAAMALLAGGLSRGLGSHPAAAGRDA
VVFWVLLLSTWCTAPARAIQVTVSNPYHVVLFPQPVLPCTYQMTSTPTQPIVIWKYKSFCDRIADAFSP
ASVDNQLNAQLAAGNPGYNPYVECQDSVRTVRVVAUTQGNAVTLGDYYQRRITITGNADLTDFDTAWGDS
GVYYCSVVAQDLQGNNEAYAELIVLGRSGVAELLPGFQAGPIEDWLFFVVVCLAAFLIFLLGICWCQC
CPHTCCCYVRCPCPDKCCCPEALYAAGKAATSGVPSIYAPSTYAHLSAKTPPPAMIPMGPAYNGYPGG
YPGDVDRSSSAGGQGSYVPLLRTDSSVASEVRSGYRIQASQQDDSMRVLYYMEKELANFDPSRPGPPSGR
VERAMSEVTSLEDDWRSRPSRGPALETPIRDEEWGHSRSPSRGWDQEAREQAGGGWRARRPRARSVDAL
DDLTPSTAEGSRSPTSNGGRSRAYMPPRSRSRDDLYDQDDSRDFRSRDPHYDDFRSRERPPADPRSHH
HRTRDPRDNGSRSGDLPYDGRLEEAVRKKGSEERRPHKEEEEAYYPPAPPPYSETDSQASRERRLKKN
LALSRESLV

MCAM (human canonical, Uniprot ID P43121-1, 646 AA, MW 71.6 kDa):

MGLPRLVCAFLLAACCCPRVAGVPGEAEQPAPELVEVEVGSTALLKGGLSQSQGNLSHVDWFSVHKEKRT
LIFRVRQGQGQSEPGYEQRLSLQDRGATLALTQVTQDTERIFLCQGKRPRSQEYRQLRVYKAPEEPNIQ
VNPLGIPVNSKEPEEVATCVRNGYPIQVIWYKNGRPLKEEKNRVIQSSQTVESSGLYTLQSILKAQLV
KEDKDAQFYCELNRYLPSGNHMKESREVTVPVFYPTEKVWLEVEPVGMLKEGDRVEIRCLADGNPPHFISI
SKQNPSTREAAEETTNDNGVLVLEPARKEHSGRYECQGLLDLTMISLLSEPQELLVNVSDVRVSPAAPER
QEGLSLTLCSEAESSQDLEFQWLREETGQVLERGPVQLHDLKREAGGGYRCVASVPSIPGLNRTQLVNVA
IFGPPWMMAFKERKVWVKENMVNLNLSCASGHPRPTISWNVNGTASEQDQDPQRVLSTLNVLVTPELLETGV
ECTASNDLGKNTSILFELVNLTTLTPDSNTTGISTASPTRANSTSTERKLPEPESRGVVIVAVIVC
ILVLAVLGAVLYFLYKKGKLPCCRSGKQEITLPPSRKSELVVEVKSDLPEEMGLLQGSSGDKRAPGDQGE
KYIDLRH

MDFI (human canonical, Uniprot ID Q99750, 246 AA, MW 25.0 kDa):

MYQVSGQRPGCDAPYGAPSAAPGPAQTLSSLPGLEVVTGUTHPAEAAPEEGSLEEAATPMPQGNGPGIPQ
GLDSTDLDVPTEAVTCQPQGNPLGCTPLPNDSGHPSLEGTRRAGNGALGGPKAHRKLOTHPSLASQGSK
KSKSSSKSTSQIPLQAQEDCCVHCILSCLFCFLTLNCIVLDCATCGSCSSEDSCLCGGCGECADC
LPCDLDGILDACCESADCLEICMECCGLCFSS

NCAM1 (human canonical*, Uniprot ID P13591-2, 858 AA, MW 94.6 kDa):

MLQTKDLIWTLFFLGTAVSLQDIVPSQGEISVGESKFLCQVAGDAKDIDSWFSPNGEKLTPNQQRISV
VWNDDSSSTLTIYNANIDDAGIYKCVVTGEDSESEATVNKIFQKLMFKNAPTPQEFREGEDAVIVCDVV
SSLPPTIWKHKGRDVILKKDVRFIVLSNNYLQIRGIKKTDEGYRCEGRILARGEINFKDIQVIVNPPT
IQARQNIVNATANLGQSVTLVCDAEGLPEPTMSWTKDGEQIEQEEDEKYIIFSDDSQLTIKKVDKNDAE
YICIAENKAGEQDATIHLKVFAKPKITYVENQTAMELEEQVTLCEASGDPIPSITWRTSTRNISSEEKAS
WTRPEKQETLDGHMVVRSHARVSSLTLKSIQYTDAGEYICTASNTIGQDSQSMYLEVQYAPKLQGPVAVYT
WEQNQVNITCEVFAYPSATISWFRDGQLLPSSNYSNIKIYNTPSASYLEVTPDSENDFGNYNCTAVNRIGQ
ESLEFILVQADTPSSPSIDQVEPYSTAQVQFDEPEATGGVPILKYKAERAVGEEVWHSKWYDAKEASME
GIVTIVGLKPETTYAVRLAALNGKGLGEISAASEFKTQPVQGEPSAPKLEGQMGEDGNSIKVNLIKQDDGG
SPIRHYLVRYRALSSSEWKPEIRLPSGSDHVMLKSLDWNAEYEVYVVAENQQGKSAAHFVFRSAQPTAIP
ANGSPTSGLSTGAIVGILIVIFVLLVVVDITCYFLNKCGLFMCIAVNLCGKAGPGAKGKDMEEGKAIFSK
DESKEPIVEVRTEEERTPNHDGGKHTEPNETTPLTEPEKGPAEKPECQETETKPPADEVKTPNDATQTK
ENENKA

*S856N point mutation relative to canonical sequence

NCSTN (human isoform 2*, Uniprot ID Q92542-2, 689 AA, MW 76.7 kDa):

MDFNLILESLCRGNVERKIVIPLNKATPCVRLLNATHQIGCQSSISGDTGVIHVVEKEEDLQWVLTDGPN
PPYMLVLESKHFTRDLMKLGRTSRIAGLAWSLTKPSPASGFSPSVQCPNDGFGVYSNSYGPFAHCREI
QWNSLGNGLAYEDSFPIFILEDENETKVIKQCYQDHNLSQNGSAPTFPLCAMQLFSMHAVISTATCMRR
SSIQSTFSINPEIVCDPLSDYNVWSMLKPINNTGTLKPDDRVAATRLDSRSFFWNVAPGAESAVASFVT
QLAAAEALQKAPDVTTLPRNMFVFFQGETFDYIGSSRMVYDMEKGKFVQLENVDSFVELGQVALRTSLE
LWMHTDPVSQNEVRNQVEDLLATLEKSGAGVPAILRRPNQSQPLPSSLQRFLRARNISGVVLADHSG
AFHNKYYQSIYDTAENINVSYPEWLSPEEDLNFVTDATAKALADVATVLGRALYELAGGTNFSDTVQADPQT
VTRLLYGLIKANNSWFQSILRQDLRSYLGDPQLQHYIAVSSPTNTVVQYALANLTGTVVNLTREQCQD
PSKVPSENKDLYEYWVQGPLHSNETDRLPRCVRSTARLARALSPAELSQWSSTEYSTWESRWKDIHAR
IFLIASKELELITLTVGFGILIFSLIVTYCINAKADVLFIAPREPGAVSY

*contains R637H point mutation relative to isoform 2

NECTIN2 (PVRL2 human isoform Alpha*, Uniprot ID Q92692-2, 479 AA, MW 51.4 kDa):

MARAAALLPSRSPTPLLWPLLLLLLETGAQDVRVQVLPEVRGQLGGTVELPCHLLPPVGLYISLVTWQ
RPDAPANHQNVAAFHPKMGSFSPPKGSERLSFVSAKQSTGQDTEAEIQLDATLALHGLTVEDEGNYTCF
ATFPKGSSVRGMMTWRVIAKPKNQAEAQKVTFSQDPTTVALCISKEGRPPARISWLSSLDWEAKETQVSGTL
AGTVTVTSRFTLVPSGRADGTVTCKVEHESFEELPVTLSVRYPPEVSISGYDDNWYLGRTDATLSCD
VRSNPEPTGYDWSTTSQFTPTSAVAQGSQLVIHAVDSLNFNTTFVCTVTNAVGMGRAEQVIFVRETPRASPR
DVGPLVWGAVGTTLLVLLLAGGSLAFILLRVRRRKSPGGAGGGASDGFFYDPKAQVLNGDGPFWTPV
VPGPMEPDGKDEEEEEEEKAEGKGLMLPPPAALEDDMESQLDGLSLISRRAVYV

*This isoform is derived from GenBank sequence AF058448 as characterized by Warner, et al.(15) and contains an alternative transmembrane domain sequence relative the canonically defined isoform, Uniprot ID Q92692-1

NPTN (human isoform 1, Uniprot ID Q9Y639-1, 282 AA, MW 31.3 kDa):

MSGSSLPSALALSLLLVSGSLLPGPGAAQNEPRIVTSEEVIRDSPVLPVTLCQCNLTSSHTLTYSWTKN
GVELSATRKNASNMEMYRINKPRAEDSGEYHCVYHFVAPKANATIEVKAAPDITGHKRSENKNEGQDATMY
CKSVGYPHPDWIWRKKENGMPMDIVNTSGRFFIINKENYTELNVNLQITEDPGEYECNATNAIGSASVVT
VLRVRSHLAPIWPFLGILAEIIILVVIIVVYEKRKRPDEVPPDDEPAGPMKTNSTNNHKDKNLQRNTN

OCLN (human canonical*, Uniprot ID Q16625-1, 522 AA, MW 59.1 kDa):

MSSRPLESPPPYRPDEFKPNHYAPSNDIYGGEMHVRPMLSQPAYSFYPEDEILHFKWTSPPGVIRILSML
IIVMCIAIFACVASTLAWDRGYGTSLLGGSGVGPYGGSGFGSYGSGYGYGYGYGYGGYTDPRAAKGFM
AMAAFCFIAALVIFTSVIRSEMSRTRYYLIVSAILGIMVIATIVYIMGVNPTAQSSGSLYGSQIY
ALCNQFYTPAATGLYVDQYSYHCVVDPQEAIIAIVLGFMIIVAFALIIFFAVKTRKMDRYDKSNILWDKE
HIYDEQPPNVEEWKNSAGTQDVSPSPSDYVERVDSPMAYSSNGKVNDKRFYPESSYKSTPVPEVVQELP
LTSPVDDFRQPRYSSGGNFETPSKRAPAKGRAGRSKRTEQDHYETDYGESCDELEEDWIREYPPITS
QQRQLYKRNFDTGLQEYKSLQSELDEINKELSRLDKELDDYREESEYMAADEYNRLKQVKGSADYKS
NHCKQLSKLSHIKMVGDYDRQKT

*L233S point mutation relative to canonical sequence

PODXL (human isoform 2, Uniprot ID O00592-2, 526 AA, MW 55.4 kDa):

MRCALALSALLLSTPPLLPSSPSPSPSQNATQTTDSSNKTAPTPASSVTIMATDTAQQSTVPTS
KA
NEILASVKATTLGVSSDSPGTTLAQQVSGPVNTTVARGGGSGNPTTTIESPKSTSADTTVATSTATAK

PNTTSSQNGAEDTTNSGGKSSHVTDLTSTKAELTTPHPTSPLSPRQPTSTHPVATPTSSGHDHLMKIS
SSSSTVAIPGYTFPSGMTTLPLSSVISQRTQQTSSQMPASSTAPSSQETVQPTSPATALRPTLPETMSS
SPTAASTTHRYPKTPSPPTVAHESNWAKCEDLETQTQSEKQLVNLNTGNTLCAGGASDEKLISLICRAVKAT
FNPAQDKCGIRLASVPGSQTVVVKEITIHTKLPAKDVTYERLKDWDLEKEAGVSDMKLGQGPPEEAEDRF
SMPLIITIVCMASFLLVAALYGCCHQRQLSQRKDQQLTEELQTVENGYHDNPTLEVMTSSEMQEKKVVS
LNGELGDSWIVPLDNLTKDDLDEEEDTHL

PTK7 (human canonical*, Uniprot ID Q13308-1, 1070 AA, MW 118.4 kDa):

MGAARGSPARPRLPLLSVLLPLGGTQTAIVFIKQPSSQDALQGRALLRCEVEAPGPVHVYWLLDGAP
VQDTERRFAQGSSLFAAVDRPQDSGTFCVARDVTGEEARSANASFNIKWIEAGPVVLKHPASEAEIQP
QTQVTLRCHIDGHPRTYQWFRDGTPSLDGQSNTVSSKERNLTLRPAGPEHSGLYSCCAHSAGFQACSSQ
NFTLSIADESFARVVLAPQDVVARYEAMFHQCFSAQPPPSLQWLFEDETPTINRSRPPHLRRATVFANG
SLLLTLQVRPRNAGIYRCIGQGQRGPIILEATLHIAEIEDMLFEPRVFTAGSEERVTCLPPKGLPEPSW
WEHAGVRLPTHGRVYQKGHELVLANIAESDAGVYCHAANLAGQRRQDVNITVATVPSWLKKPQDSQLEEG
KPGYLDCLTQATPKPTVVWYRNQMLISEDSRFEVKNGTLRINSVEVDGTWYRCMSSTPAGSIEAQARVQ
VLEKLKFTPPPQPPQCMEDKEATVPCSATGREKPTIKWERADGSSLPEWVTDNAGTLHFARVTRDDAGNY
TCIASNGPQGQIRAHVQLTVAVFITFKEPERTTVYQGHTALLQCEAQGDPKPLIQWKGKDRILDPTKLGP
RMHIFQNGSLVIHDVAPEDSGRYTCIAGNSCNIKTEAPLYVVDKPVPEESEGPGSPPYKMIQTIGLSVG
AAVAYIIAVLGLMFYCKRKCKAKRLQKPEGEPEMECLNGGPLQNGQPSAEIQEEVALTSLSGSGPAATNK
RHSTSDFMHPRSSLQPIITLGKSEFGEVFLAKAQGLEEGVAETLVLVKSLSQSKDEQQQLDFRRELEMFGK
LNHANVVRLLGLCREAEPHYMVLEYVDLGDLKQFLRISKSKDEKLKSQPLSTKQVALCTQVALGMEHLSN
NRFVHKDLAARNCLVSAQRQVKVSALGLSKDVNSEYYHFQAWVPLRWMSPEAILEGDFSTKSDVWAFCV
LMWEVFTHGEMPHGGQADDEVLAQAGKARLPQPEGCPSKLYRLMQRCWALSPKDRPSFSEIASALGDST
VDSKP

*L93P point mutation relative to canonical sequence

PTPRF (human isoform 2*, Uniprot ID P10586-2, 1898 AA, MW 211.7 kDa):

MAPEPAPGRTMVPVLPALVMLGLVAGAHGDSKPVFIKVPEQDTGLSGGVASFVCQATGEPKPRITWMKKKGK
KVSSQRFEVIEFDGAGSVLRIQPLRVQRDEAIYECTATNSLGEINTSAKLSVLEEEQLPPGPSIDMGPQ
LKVEKARTATMLCAAGGNPDPEISWFKDFLPVDPATSNGRIKQLRSGALQIESSEESDQGKYECVATNSA
GTRY SAPANLYVRVRRVAPRFSI PPPSSQEVMPGGSVNLTCVAVGAPMPYVKWMMGAEELTKEDEMPVGRNV
LELSNVRSANYTCVAISSLGMIEATAQVTVKALPKPIDLVTETTATSVTLTWDSGNSEPVYYGIQYR
AAGTEGPFQEVDGVATTRYSIGGLSPFSEYAFRVLAVNSIGRGPPSEAVRARTGEQAPSSPPRRVQARMLS
ASTMLVQWEPPPEEPNGLVRGYRVYYTPDSRRPPNAWHKHNTDAGLTTVGSLLPGITYSLRVLAFTAVGDG
PPSPTIQVKTQQGVPAQPADFQAEVESDTRIQLSLLPPQERIIMYELVYWAEEDEDQHQKVTFDPTSSYT
LEDLKPDLYRFQLAARSMDMGVGVFTPTIEARTAQSTPSAPPQKVMCVMSGTTVRSWVPPADS RNGVI
TQYSVAYEAVDGEDRGRHVVDGISREHSSWDLVGLEKWTYRVWVRAHTDVGPGPESSPVLVRTDEDVPSG
PPRKVEVEPLNSTAVHVYWKLPVPSKQHGQIRGYQVTYVRLENGEPRLPPIIQDVMLAEAQETTISGLTPE
TTYSVTVAAYTTKGDGARSKPKIVTTGAVPGRPTMMISTTAMNTALLQWHPPKELPGELGYRLQYCRAD
EARPNTIDFGKDDQHFTVTGLHKGTTYIFRLAAKNRAGLGEFEKEIRTPEDLPSGFPQNHLVTGLTTSTT
ELAWDPPVLAERNGRIISYTVVFRDINSQQUEEPEMLWVTGPVLAVILIIILIVIAILLFKRK
RTHSPSSKDEQSISGLKDSLHSSDPVEMRRLNYQTPGMRDHPPPIPTDLADNIELKANDGLKFSQYES
IDPGQQFTWENSNLEVNPKNRYANVIAYDHSRVLTSIDGVPGSDYINANYIDGYRKQNAYTATQGPLPE
TMGDFWRMVWEQRTATVMMTRLEEKSRVKCDQYWPARGETCGLIQVTLDDTVELATYTVRTFALHKSGS
SEKRELRFQFMAWPDHGVPYEYPTPILAFLLRVKACNPLDAGPMVVCAGVGRGCFIVIDAMLERMKHE
KTVDIYGHVTCMRSQRNYMVQTEDQYVFIREALLEAATCGHTEVPARNLYAHIQKLGVPPGESVTAMELE
FKLASSKAHTSRFISANLPCNKFKNRLVNIMPYELTRVCLQPIRGVEGSDYINASFLDGYRQKAYIATQ
GPLAESTEDFWRMLWEHNSTTIVMLTKLREM GREKCHQYWPAERSARYQYFVVDPMAEYNMPQYIILREFKV

TDARDGQSRTIRQFQFTDWPEQGVPKTGEFIDFIGQVHKTKEQFGQDGPITVHCSAGVGRGVFITLSIV
LERMRYEGVVDMFQTVKTLRTQRPAMVQTEDQYQLCYRAALEYLGSFDHYAT

***I1412T point mutation relative to isoform 2 sequence; Δ772–780 relative to canonical sequence**

PVR (human canonical*, Uniprot ID P15151-1, 417 AA, MW 45.3 kDa):

MARAMAAAWPLLVALVLWSPPPGTGDVVVQAPTQVPGFLGDSVTLPACYLQVPNMEVTHVSQLTWARHGE
SGSMASFHFQTQGPSSYSESKRLEFVAARLGAEELRNASLRMFGRLVEDEGNYTCLFVTPQGSRSVDIWLRLV
AKPQNTAEVQKVQLTGEPVPMARCVSTGGRPPAQITWHSDLGGMPNTSQVPGFLSGTVTVTSILWILVPSSQ
VDGKNVTCKVEHESFEKPQLTVNLTVYYPPPEVSISGYDNNWYLGQNEATLTCARSNPETGYNWSTTMG
PLPPFAVAQGAQLLIRPVDKPINTTLCNVTNALGARQAEITVQVKEGPPSEHGMRSNAIIFLVLGILVF
LILLGIGIYFYWSKCSREVLWHCHLCPSTEHASASANGHVSYSAVSRENSSSQDPQTEGTR

***contains I340M point mutation relative to canonical (natural variant UniProtKB/Swiss-Prot: VAR_011736)**

RTN4R (human canonical, Uniprot ID Q9BZR6, 473 AA, MW 50.7 kDa):

MKRASAGGSRLLAWVLWLQAWQVAAPCPGACVCYNEPKVTTSCPQQGLQAVPGVIPAASQRIFLHGNRISH
VPAASFRACRNLTILWLHSNVLARIADAATGLALLEQLDSLNAQLRSVDPATFHGLGRLHTLHLDRCGL
QELGPGLFRGLAALQYLYLQDNALQALPDDTFRDGLNLTHFLHGNRISSVPERAFRGLHSIDRLLLHQNR
VAHVHPHAFRDLGRLMTLYLFANNLSALPTEALAPLRALQYLRNNDNPWCDCRARPLWAWLQKFRGSSSE
VPCSLPQRLLAGRDLKRLAANDLQGCAVATGPYHPIWTGRATDEEPLGLPKCCQDAADKASVLEPGRPASA
GNALKGRVPPGDSPPNGNSGPRHINDSPFGTLPGSAEPPLTAVRPEGSEPPGFPTSGPDRRGCSRKNRTR
SHCRLGQAGSGGGGTGDSEGGALPSLTCSTPLGLALVLWTVLGPC

SMPDL3B (human isoform 2, Uniprot ID Q92485-2, 373 AA, 41.7 kDa):

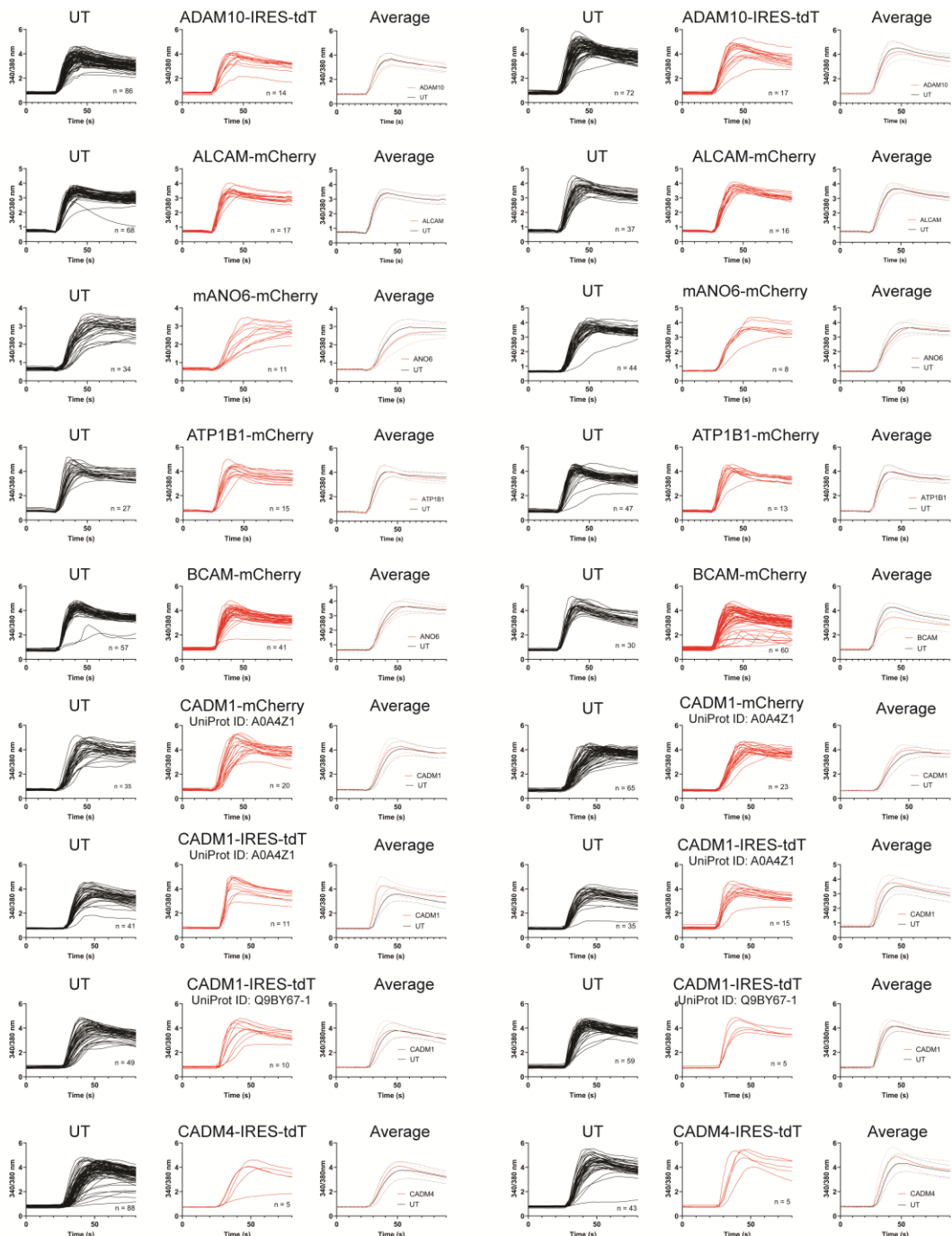
MRLLAWLIFLANWGGARAEPGKFWHIADLHLDPDYKVSKDPFQVCPSPAGSQPVDPAGPWGDYLCDSPWALI
NSSIYAMKEIEPEPDFILWTGDDTPHVPDEKLGEAAVLEIVERLTKLIREVFPDTKVAALGNHDFHPKNQ
FPAGSNNIYNQIAELWKPWLSNESIALFKKGAFYCEKLPGPMSGAGRIVVLNTNLYYTSNALTADMADPGQQ
FQWLEDVLTDAKAGDMVYIVGHVPPGFFEKTNKAWFREGFNEKYLKVVVKHRVIAGQFFGHHTDSFR
MLYDDAGVPISAMFITPGVTPWKTTPGVVNGANNPAIRVFYDRATLSKVRSPAEEARGGGWEGLKCITT
FPHSQLIHLPLTTEPQEG

TMEM30A (human isoform 2, Uniprot ID Q9NV96-2, 325 AA, MW 36.7 kDa):

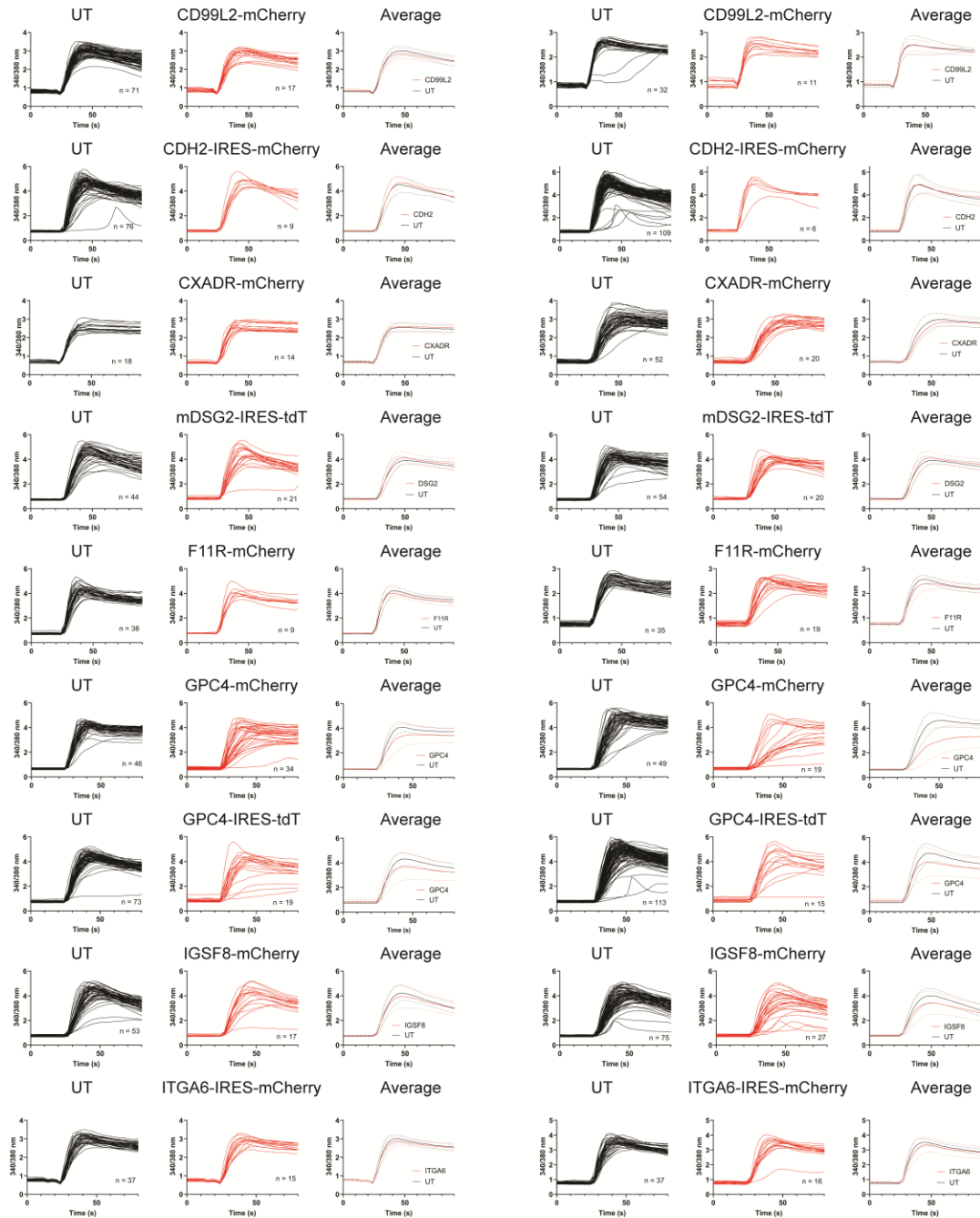
MAMNYNAKDEVDGPPCAPGGTAKTRRPDNTAFKQORLPAWQPILTAGTVLPIFFIIGLIFIPIGIGIFVT
SNNIREIEGNVFMYYGLSNFYQNHRRYVKSRDDSQLNGDSSALLNPSKECEPYRRNEDKPIAPCGAIANSM
FNDTLELFLIGNDSYPIPIALKKKGIAWWTDKNVKFRNPPGDNLEERFKGTTKPVNWLKPVYMLSDPDN
NGFINEDFIVWMRTAALPTFRKLYRLIERKSDLHPTLPAGRYSLNVTYNYPVHYFDGRKRMILSTISWMGG
KNPFLGIAYIAVGSIISFLLGVVLLVINHKYRNSSNTADITI

Appendix III: Calcium imaging screen representative data for each candidate gene, alphabetically, showing the Yoda1 response with two representative trials on the left and right. Cells without visible transfection (UT, black traces) are being compared to those with visible red fluorescence (red traces) in the same field of view, together with an overlay of the average \pm SD, as described in the Materials and Methods. Genes are C-terminally fused to mCherry unless otherwise noted (tdT = tdTomato). See Appendix II for cDNA and protein sequences that were used. If applicable (e.g., if multiple constructs for the same gene were tested), the corresponding UniProt ID is noted. Cells were excluded from analysis if they were obviously unhealthy (round morphology or baseline calcium ratio >1.5), did not respond to Yoda1 within the first 10 s of application and/or did not show green PIEZO1-GFP fluorescence, or did not respond to ionomycin following the Yoda1 stimulus. In a few cases, very few transfected cells remained in the field of view, either due to poor transfection efficiency, expression, or cell health issues resulting from transient overexpression. This has been noted in Appendix II.

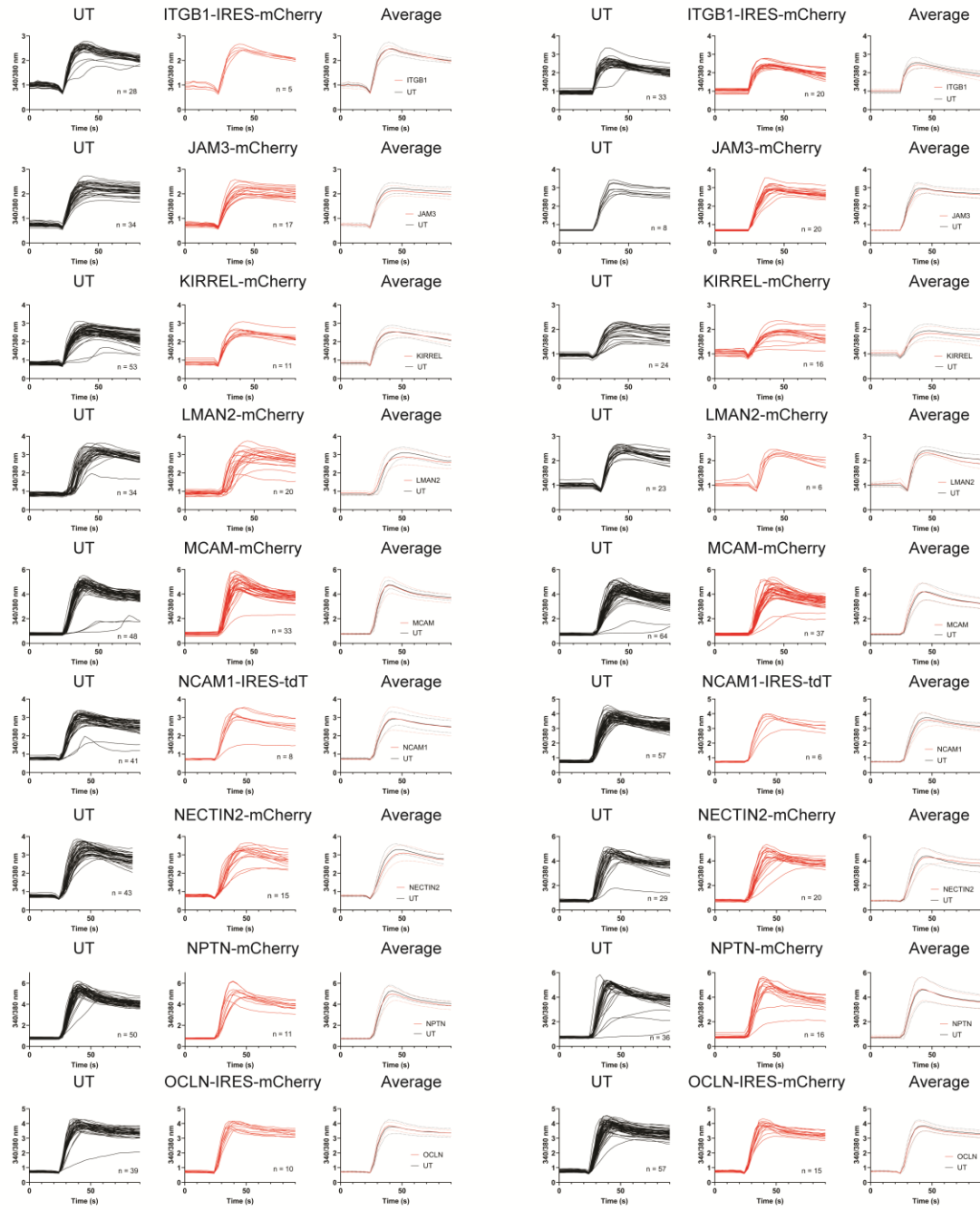
Appendix III, continued:



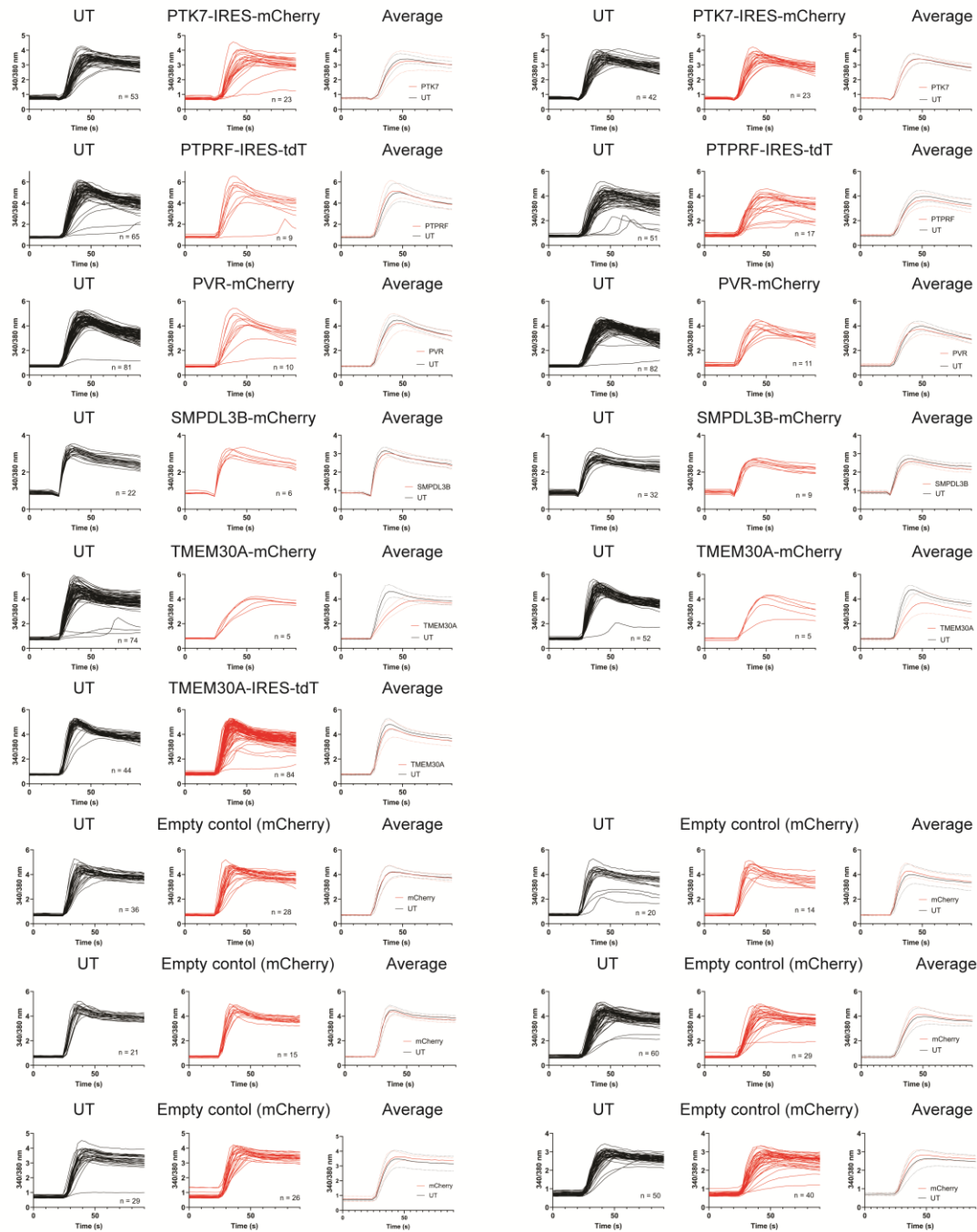
Appendix III, continued:



Appendix III, continued:



Appendix III, continued:



Supplementary File 2 (separate file). PIEZO1 interactome in the HEK293F PIEZO1 stable cell line, showing all proteins identified in a single multiplexed TMT proximity labeling dataset prior to any filtering ('PIEZO1 interactome, HEK stable' tab). The final 185 high-confidence proteins shown in Fig. 1 are listed in the 'Final 185 proteins' tab (3 separately treated biological replicates for each condition).

How to read this spreadsheet:

TMT1–3 are 3 biological replicates performed with a DMSO vehicle control, while TMT4–6 are 3 biological replicates performed in the presence of 10 μ M Yoda1 agonist (~1–2-min. application). Normalized signal from each TMT channel is indicated for each protein in columns F–K (Sum of TMT1–6 = 100%). Column M is the ratio of average signal coming from TMT4–6 (Yoda1)/ the average from TMT1–3 (DMSO control) and is illustrated in Fig. S1, E.

Color coding indicates which proteins were omitted with each filter and why:

- Yellow highlight (Columns A–M): Eliminated because spectral count (Column D) was <5 (our cutoff for reliable protein ID)
- Red text (Columns A–M): Eliminated because the protein was not captured in all four TMT datasets in HEK cells (3 with transient overexpression, 1 with the stable cell line, representing 9 total biological replicates). If a protein was not seen in all 4 independent TMT experiments, this is indicated by a 'FALSE' in column 'L'). Columns Y–AA indicate whether a protein was captured ('TRUE') or not ('FALSE') in each of three transient PIEZO1 overexpression TMT datasets in HEK cells in addition to the stable cell line.
- Blue text (Columns A–M): Eliminated because the protein was equally enriched by PIEZO1 lacking a BBS tag (these are primarily endogenous biotin-associated proteins that were captured during pull-down with streptavidin)
- Red text (Columns R–V): Eliminated because the protein is present in >25% (179/716) of CRAPome datasets. Column T indicates this number out of 716. Column W indicates which of the CRAPome filtered proteins are annotated to be intracellular or cytoplasmic (Y = YES, N = NO) based on GO analysis (<https://geneontology.org/>)^(16, 17) and the Human Protein Atlas (<https://www.proteinatlas.org/>)⁽⁶⁾, which suggests they are coming from dead cells and debris instead of specific labeling on the cell surface.

*Note: *Mouse* PIEZO1-BBS (cap) is being stably expressed in a *human* cell line; therefore, peptide quantification for PIEZO1 (due to self-labeling) appears lower than would be expected for this type of experiment (only common tryptic peptides between mouse and human PIEZO1 are being counted). Using a mouse proteome search algorithm instead of human for this same dataset, PIEZO1 goes from 4.4% sequence coverage (spectral count 36) up to 25.25% sequence coverage (spectral count 177), indicating that this difference is only due to species.

SI References

1. E. W. Deutsch, *et al.*, The ProteomeXchange consortium at 10 years: 2023 update. *Nucleic Acids Res* **51**, D1539–D1548 (2023).
2. Y. Perez-Riverol, *et al.*, The PRIDE database resources in 2022: a hub for mass spectrometry-based proteomics evidences. *Nucleic Acids Res* **50**, D543–D552 (2022).
3. J. Wu, R. Goyal, J. Grandl, Localized force application reveals mechanically sensitive domains of Piezo1. *Nat Commun* **7**, 12939 (2016).
4. K. H. Loh, *et al.*, Proteomic Analysis of Unbounded Cellular Compartments: Synaptic Clefts. *Cell* **166**, 1295-1307.e21 (2016).
5. E. V. Vinogradova, *et al.*, An Activity-Guided Map of Electrophile-Cysteine Interactions in Primary Human T Cells. *Cell* **182**, 1009-1026.e29 (2020).
6. P. J. Thul, *et al.*, A subcellular map of the human proteome. *Science* **356**, eaal3321 (2017).
7. B. Coste, *et al.*, Piezo1 and Piezo2 are essential components of distinct mechanically activated cation channels. *Science* **330**, 55–60 (2010).
8. A. H. Lewis, J. Grandl, Mechanical sensitivity of Piezo1 ion channels can be tuned by cellular membrane tension. *eLife* **4**, e12088 (2015).
9. A. Spandidos, X. Wang, H. Wang, B. Seed, PrimerBank: a resource of human and mouse PCR primer pairs for gene expression detection and quantification. *Nucleic Acids Research* **38**, D792–D799 (2010).
10. A. Spandidos, *et al.*, A comprehensive collection of experimentally validated primers for Polymerase Chain Reaction quantitation of murine transcript abundance. *BMC Genomics* **9**, 633 (2008).
11. X. Wang, B. Seed, A PCR primer bank for quantitative gene expression analysis. *Nucleic Acids Res* **31**, e154 (2003).
12. Z. Zhou, *et al.*, MyoD-family inhibitor proteins act as auxiliary subunits of Piezo channels. *Science* **381**, 799–804 (2023).
13. C. Wu, X. Jin, G. Tsueng, C. Afrasiabi, A. I. Su, BioGPS: building your own mash-up of gene annotations and expression profiles. *Nucleic Acids Research* **44**, D313–D316 (2016).
14. A. Gschwind, S. Hart, O. M. Fischer, A. Ullrich, TACE cleavage of proamphiregulin regulates GPCR-induced proliferation and motility of cancer cells. *EMBO J* **22**, 2411–2421 (2003).
15. M. S. Warner, *et al.*, A cell surface protein with herpesvirus entry activity (HveB) confers susceptibility to infection by mutants of herpes simplex virus type 1, herpes simplex virus type 2, and pseudorabies virus. *Virology* **246**, 179–189 (1998).
16. M. Ashburner, *et al.*, Gene Ontology: tool for the unification of biology. *Nat Genet* **25**, 25–29 (2000).
17. The Gene Ontology Consortium, *et al.*, The Gene Ontology knowledgebase in 2023. *Genetics* **224**, iyad031 (2023).

